AD NUMBER

AD253970

LIMITATION CHANGES

TO:

Approved for public release; distribution is unlimited.

FROM:

**Distribution authorized to U.S. Gov't. agencies and their contractors;
Administrative/Operational Use; FEB 1961. Other requests shall be referred to Office of Naval Research, 875 North Randolph Street, Arlington, VA 22203-1995.**

AUTHORITY

ONR ltr, 28 Jul 1977

AEROELASTIC AND STRUCTURES RESEARCH LABORATORY
MASSACHUSETTS INSTITUTE OF TECHNOLOGY

TECHNICAL REPORT 75-2

SIMILARITY LAWS REQUIRED FOR EXPERIMENTAL AEROTHERMOELASTIC STUDIES PART 2 — HYPERSONIC SPEEDS

BY
JOHN M. CALLIGEROS
JOHN DUGUNDJI

FOR THE
OFFICE OF NAVAL RESEARCH
DEPARTMENT OF THE NAVY
CONTRACT NO. NONR-1841(46)

FEBRUARY 1961

AEROELASTIC AND STRUCTURES RESEARCH LABORATORY
MASSACHUSETTS INSTITUTE OF TECHNOLOGY

TECHNICAL REPORT 75-2

SIMILARITY LAWS REQUIRED FOR EXPERIMENTAL AEROTHERMOELASTIC STUDIES
PART 2 -- HYPERSONIC SPEEDS

By

JOHN M. CALLIGEROS
JOHN DUGUNDJI

FOR THE
OFFICE OF NAVAL RESEARCH
DEPARTMENT OF THE NAVY
CONTRACT NO. Nonr-1841(46)

FEBRUARY 1961

TABLE OF CONTENTS

ABSTRACT

The similarity laws for the experimental study of aerothermoelastic phenomena associated with flight at hypersonic Mach numbers are derived. This study considers in detail the parameters associated with the external pressure and heat flux imposed on the structure, the heat transfer distribution within the structure (for both ablating and non-ablating materials) and the stress-deflection behavior under short-time and long-time loading conditions. The structural parameters associated with nonlinear material properties at high temperatures, plasticity, creep and fatigue are briefly considered.

Similitude for the general aerothermoelastic problem is possible only for a scale ratio of one and for a thermal and pressure environment identical with the prototype. The basic conflict arises when mutually satisfying the requirements of same temperature, Reynolds number, surface radiation parameter $\epsilon_o T_o^3 L/K_o$ and the aeroelastic parameter $\rho_\infty U^2/E_o$.

Means of dealing with this conflict are suggested. These include looking at more specialized situations peculiar to both blunt bodies and affinely related slender bodies in continuum and free molecule flow, the use of "incomplete aerothermoelastic testing" in which pressure and thermal loadings are estimated in advance and applied artificially to the model, and the use of "restricted purpose" tests investigating a particular facet of the complete aerothermoelastic problem.

Finally, a survey of some available types of test facilities appropriate for these investigations is given.

LIST OF FIGURES

LIST OF PRINCIPAL SYMBOLS

a_e	Accomodation coefficient
C	Plate extensional stiffness per unit length, $\int_{-\delta/2}^{\delta/2} \frac{E}{1-\nu^2}\, dz$
c	Chord
C_p	Specific heat of body material
c_p	Specific heat of gas at constant pressure
D	Plate bending stiffness per unit length, $\int_{-\delta/2}^{\delta/2} \frac{Ez^2}{1-\nu^2}\, dz$; diffussion coefficient
d	Typical nose dimension
E	Young's Modulus
f_1	$\int_0^{\bar{T}} \bar{c}_p\, d\left(\frac{T}{T_s}\right)$
F	Stress function
f	Fraction of molecules diffusely reflected
g	Acceleration due to gravity
h	Enthalpy per unit mass
H_{eff}	Effective energy absorbed per unit mass of ablated material, $q_A/\dot{m}_L$
K	Heat conductivity of body material
k	Heat conductivity of gas; nose drag coefficient
K_n	Knudsen number, λ/L
L	Characteristic length
L_e	Lewis number, $\rho c_p D/k$
L_m	Heat of fusion per unit mass

L_v	Heat of vaporization per unit mass
M_∞	Free stream Mach number
m	Mass per unit area
M_T	Midplane thermal moment per unit length, $\int_{-\delta/2}^{\delta/2} \frac{E\alpha\Delta T z}{1-\nu}\, dz$
$\dot{m}$	Mass ablation rate
N_T	Midplane thermal force per unit length, $\int_{-\frac{\delta}{2}}^{\delta/2} \frac{E\alpha\Delta T}{1-\nu}\, dz$
p	Pressure
P_r	Prandtl number $\mu c_p/k$
P_{r_s}	Stagnation Prandtl number $\mu_s c_{ps}/k_s$
q	Heat flux per unit area
R	Body nose radius of curvature; universal gas constant
R_e	Reynolds number $\rho UL/\mu$
R_{e_s}	Stagnation Reynolds number, $\rho_\infty UL/\mu_s$
r	Polar coordinate
S	Molecular speed ratio, $M_\infty\sqrt{\gamma/2}$
$\dot{s}$	Ablation velocity, $\dot{m}_L/\rho_L$
t	Time
T	Temperature
U	Free stream velocity
u, v, w,	Velocity components; displacement components
V_o	Reference velocity associated with molten layer
x, y, z,	Rectangular coordinates

α	Coefficient of thermal expansion
β	Local angle of attack
γ	Ratio of specific heats
δ	Thickness
ϵ	Emissivity; strain
η	Vapor injection empirical factor
π	Thermal diffusivity, $K/\rho c_p$
λ	Molecular mean free path
μ	Viscosity of gas
ν	Poisson's ratio
ρ	Density
σ	Normal stress component; Stefan-Boltzman Constant
$\sigma_{.7}$	Stress corresponding to secant modulus of .7E.
τ	Thickness ratio; shear stress
$\bar{\chi}$	Viscous interaction parameter, $M_\infty^3\sqrt{C}/\sqrt{R_{e_\infty}}$

Subscripts

A	Of aerodynamic origin
B	Body
ear	Earth
F	Of nonaerodynamic origin
i	Gas-liquid interface
L	Pertaining to melt layer

M	Model; melting point value
0	Reference value
P	Prototype
s	Pertaining to stagnation point in external flow
sol	Solar
Ult	Ultimate
v	Pertaining to vaporization process
w	Value at body surface
∞	Free stream value

1. INTRODUCTION

The present report constitutes the second phase of a study concerned with the similarity laws required for experimental aerothermoelastic studies. The first phase was primarily concerned with flight Mach numbers extending into the higher supersonic range ($M \leq 3.5$) and with maximum structural temperatures of approximately $1000^{o}F$. Materials with elastic stress-strain properties only were considered and structural radiation was assumed negligible. The area of interest of this first phase was restricted to region I of Figure 1 and the results are presented in Ref. 1. It was found that the basic similarity parameters for combined aerodynamic, heat transfer and stress deflection studies are the free stream Reynolds number Re_{∞}, Mach number M_{∞} and the basic aeroelastic parameter P_{∞}/E_{o}.

In the present report the similarity requirements associated with Mach numbers extending into the hypersonic range, regions II and III of Fig. 1, are considered. Essentially the basic ideas of similarity and non-dimensionalization of Ref. 1 are utilized and extended to cover these cases. Some of the assumptions made there are no longer applicable. The higher temperatures associated with hypersonic flight introduce new and considerably more complex phenomena relating to aerodynamic, material, and structural characteristics. The similarity laws pertaining specifically to hypersonic pressure and heat transfer similarity must now be investigated. Such additional phenomena as real gas effects, structural radiation, material ablation, nonlinear behavior of material properties at high temperatures, plasticity, creep and fatigue are also to be considered now.

This current study will first discuss in detail the parameters associated with the aerodynamic pressure distribution, aerodynamic heat transfer, heat conduction for non-ablating and ablating bodies, and the stress-deflection behavior at high speeds and temperatures. The possibility of mutually simulating the combined aerodynamic, heat transfer, and structural behavior problem will then be discussed. Again as in Ref. 1, some basic conflicts will arise, and wherever possible, some means of alleviating them will be discussed. Applications will then be made to both boost glide and ballistic type vehicles. Finally, some of the current research facilities available for testing these aerothermoelastic models will be described.

2. AERODYNAMIC SIMILARITY

2.1 General Features

The two aerodynamic quantities of primary importance in aerothermoelastic modeling are the pressure distribution and the heat transfer rate imposed on the structure by the external flow. The general similarity parameters relating to these aerodynamic quantities were obtained in a previous report, Ref. 1, for flight extending into the supersonic range ($M \leq 3.5$). It was shown there that if the following non-dimensional quantities

$$\bar{\rho} = \frac{\rho}{\rho_\infty} \quad , \quad \bar{p} = \frac{p}{p_\infty} \quad , \quad \bar{T} = \frac{T}{T_0}$$

$$\bar{u} = \frac{u}{U} \quad , \quad \bar{x} = \frac{x}{L} \quad , \quad \bar{t} = \frac{t}{t_0} \quad , \tag{2.1}$$

$$\bar{\bar{\mu}} = \frac{\mu}{\mu_\infty} \quad , \quad \bar{\bar{c}}_p = \frac{c_p}{c_{p_\infty}} \quad , \quad \bar{\bar{k}} = \frac{k}{k_\infty}$$

were introduced into the general equations of motion of a compressible, viscous, heat-conducting perfect gas, the following main similarity parameters would result,

$$M_\infty \, , \; Re_\infty \, , \; Pr_\infty \, , \; \gamma \, , \; \frac{T_0}{T_\infty} \, , \; \frac{Ut_0}{L} \, , \tag{2.2}$$

$$\text{same geometry} \, , \; \bar{\bar{\mu}} \, , \; \bar{\bar{c}}_p \, , \; \bar{\bar{k}}$$

If the above similarity parameters were made the same for both model and prototype, the non-dimensionalized equations of motion would be identical for both, and would therefore have identical solutions for the unknowns $\bar{\rho}$, $\bar{p}$, $\bar{T}$, $\bar{u}$, etc. Hence measurements of $\bar{\rho}$, $\bar{p}$, $\bar{T}$, $\bar{u}$ etc. on a

model can then be used to find ρ, p, T, u on the prototype by application of Eqs. (2.1). Therefore aerodynamic similarity in both pressure distribution and heat transfer will prevail if the similarity parameters of Eq. (2.2) are maintained equal for both model and prototype. Further, it was indicated in Ref. 1 that M_∞, and to a lesser extent γ, are (provided Re_∞ is sufficiently large) the principal parameters for pressure distribution similarity, while Re_∞ and to a lesser extent Pr_∞, are the principal heat transfer parameters. The unsteady term Ut_0/L and the reference temperature ratio T_0/T_∞, serve to define the reference time t_0 and the reference temperature T_0, respectively. The remaining parameters $\bar{\bar{\mu}}$, $\bar{\bar{c}}_p$, $\bar{\bar{k}}$ require that the variations of μ, c_p, k with temperature be of the same form for model and prototype, and are readily met in the range up to 1000°F.

At much higher Mach numbers, when one gets into the hypersonic speed range, an important new property comes into play, namely, the Mach Number Independence Principle discussed by Hayes and Probstein in Ref. 2. This states that at a sufficiently large free stream Mach number M_∞ the flow over a body becomes independent of M_∞. Considering the same general equations of motion of a compressible, viscous, heat-conducting, perfect gas as given for the supersonic case in Ref. 1, one now finds it convenient to match conditions at the stagnation point and to non-dimensionalize with respect to stagnation point rather than free stream

quantities (except for ρ and u) as follows,

$$\bar{\rho} = \frac{\rho}{\rho_\infty}\,, \quad \bar{p} = \frac{p}{p_s}\,, \quad \bar{T} = \frac{T}{T_0}\,, \quad \bar{u} = \frac{u}{U}\,,$$
$$\bar{x} = \frac{x}{L}\,, \quad \bar{y} = \frac{y}{L}\,, \quad \bar{t} = \frac{t}{t_0}\,, \tag{2.3}$$
$$\bar{\bar{\mu}} = \frac{\mu}{\mu_s}\,, \quad \bar{\bar{c}}_p = \frac{c_p}{c_{p_s}}\,, \quad \bar{\bar{k}} = \frac{k}{k_s}$$

Introducing these into the equations of motion as was done in Ref. 1, and noting the following stagnation point approximations* for high M_∞ flow,

$$p_s \approx \frac{(\gamma+3)}{2(\gamma+1)}\,\rho_\infty U^2$$
$$\rho_s \approx \frac{\gamma(\gamma+3)}{(\gamma-1)(\gamma+1)}\,\rho_\infty \tag{2.4}$$
$$h_s \approx U^2/2$$
$$T_s \approx \frac{U^2}{2\,c_{p_s} f_1}$$

one obtains then the following main similarity parameters for the hypersonic flow of a perfect gas,

$$Re_s\,,\ Pr_s\,,\ \gamma\,,\ T_0/T_s\,,\ Ut_0/L\,,\ \text{same geometry}$$
$$\bar{\bar{\mu}},\quad \bar{\bar{c}}_p\,,\quad \bar{\bar{k}} \tag{2.5}$$

where $Re_s \equiv \rho_\infty UL/\mu_s$ and $Pr_s \equiv c_{p_s}\mu_s/k_s$.

*The factor $f_1 = \int_0^1 \bar{\bar{c}}_p\, d\left(\frac{T}{T_s}\right)$ accounts for variations in c_p . For c_p = constant, $f_1 = 1$. If $\bar{\bar{c}}_p$ is simulated, then f_1 , will also be the same for both model and prototype in the above perfect gas equations.

Comparing the above with the previous similarity parameters of Eq. (2.2), it is seen that the dependence on the Mach number M_∞ has been dropped. This was made possible by the high M_∞ approximations of Eq. (2.4), which carry the implication that the free stream quantities p_∞ and T_∞ are very much smaller than the corresponding stagnation point quantities p_s and T_s, and hence can be neglected in comparison. Also it is seen that the T_0/T_s condition for the reference temperature T_0 replaces the previous T_0/T_∞ condition of Eq. (2.2). In the similarity parameters of Eq. (2.5), the R_{e_s} again is associated with viscous and heating effects, and can be neglected when considering pressure distribution similarity around blunt bodies. For slender bodies however, there appears to be a viscous interaction between the thickness of the boundary layer and the external non-viscous flow at these high Mach numbers, and the R_{e_s} condition does play a role in the aerodynamic pressure distribution similarity here. Of the remaining parameters, it is to be noted that although the Prandtl number P_r can be assumed fairly constant over a wide temperature range, the simulation of $\bar{c}_p$, $\bar{\mu}$, $\bar{k}$ is somewhat more difficult over these extended temperature ranges associated with high Mach numbers. As mentioned in Ref. 1 though, any gas whose c_p, μ and k properties can be represented by the form T^α will satisfy the conditions on $\bar{c}_p$, $\bar{\mu}$ and $\bar{k}$. Of course operating with the same gases at the same temperatures for both model and prototype will also insure simulation of these quantities.

The special case of slender affinely related bodies will be treated more in detail subsequently in Section 2.2. It will turn out there that further relaxations in similarity can be made for these slender bodies

provided the parameter $M_\infty \tau$ is large, where τ is the thickness ratio of the profile.

Thus, for general hypersonic similitude of a perfect gas, a relaxation of the Mach number condition is possible if M_∞ is sufficiently large. It is interesting to notice that for very low speeds (incompressible flow) as well as for these hypersonic speeds, the Mach number again ceases to be an important similarity parameter in aerodynamic flow.

A survey of hypersonic flow problems is given in Refs. 3 and 4. Aside from the Mach Number Independence Principle, the distinguishing features of this flow regime are the closeness of the leading edge shock wave to the body surface and the attendant high temperatures which may result in real gas phenomena. The closeness of the shock wave to the surface has enabled the flow to be treated as Newtonian, particularly over a blunt nosed body, in which case the flow characteristics become independent of M_∞. This is another manifestation of the Mach Number Independence Principle. For a slender body this closeness of the shock wave may result in an interaction with the viscous boundary layer inducing higher pressures and heat transfer rates, and requiring consideration of Reynolds number R_{e_s} effects on the pressure distribution.

The real gas phenomena assume importance at the high temperatures associated with $M_\infty > 7$ (for air), and involve consideration of dissociation and recombination processes and their associated relaxation times. They affect mainly the heat transfer rather than the pressure distribution similarity. To simulate these real gas effects, it is essential at least to maintain identical temperatures

in identical gases over model and prototype. From Eqs. (2.3) and (2.4), this requires the free stream velocity U to be maintained the same for both model and prototype, and hence the parameter U is added to the group given in Eq. (2.5). For more accurate simulation of real gas effects, it is desirable to maintain identical pressures as well as identical temperatures over model and prototype, thus assuring that the gas is in the same state for model and prototype. It is then seen from Eqs. (2.3) and (2.4), that the free stream density ρ_∞ as well as U should be maintained similar for model and prototype. This, however, causes difficulty in fulfilling the Reynolds number similarity condition.

The similarity parameters associated with hypersonic phenomena will be considered in more detail in the following sections with regard to aerodynamic pressure and heat transfer similitude individually. This separation is made possible by the Prandtl boundary layer concept. By looking at specialized situations, it will be seen that it is possible to provide further relaxations of the general conditions for supersonic flow, Eq. (2.2), and of the general conditions for hypersonic flow, Eq. (2.5).

2.2 Aerodynamic Pressure Distribution Similarity

a) Blunt Bodies

At high Mach numbers, the flow over the nose of a blunt body may be treated as Newtonian and the pressure expressed as (Ref. 3)

$$\frac{p}{p_s} \approx \sin^2\beta \tag{2.6}$$

where β is the angle between U and a surface element (local angle of attack)*. For M_∞ greater than about 3,

$$p_s \approx \frac{1}{2}\rho_\infty U^2 \frac{(\gamma+3)}{(\gamma+1)} \tag{2.7}$$

Tests reported in the literature have shown that this insensitivity to Mach number is valid for M_∞ as low as 3. Thus the pressure distribution over the nose of a blunt body may be adequately simulated by reproducing only the same geometry (β), provided both model and prototype operate above $M_\infty > 3$. The above relations also follow from application of the Mach Number Independence Principle which led to the parameters given in Eq. (2.5). Since the viscous boundary layer does not affect the pressure distribution in the neighborhood of such blunt bodies, the Re_s and P_{r_s} conditions can be disregarded. The γ condition is here absorbed in the definition of the stagnation pressure, while the Ut_o/L condition can be neglected if the flow is assumed steady. Further, the pressure distribution

---

* β includes the instantaneous velocity of the boundary as well as the instantaneous slope in its definition.

is not much affected by real gas phenomena here--any real gas effects are manifested in a decrease in the value of γ (from 1.4 to about 1.2 for air) which alters the stagnation pressure Eq. (2.7) only slightly.

b) Sharp-Nosed Slender Bodies

The hypersonic similarity rules for sharp nosed slender bodies of similar shape in inviscid flow have been developed in Refs. 5 and 6. For a family of affinely related slender bodies of thickness ratio τ in an inviscid perfect gas hypersonic flow, the pressure may be expressed as

$$\frac{p - p_\infty}{\frac{1}{2}\rho_\infty U^2} = \tau^2 \Pi \left(x/L ; M_\infty \tau, \gamma, u_0/L\tau, Ut_0/L \right) \qquad (2.8)$$

where Π is a function of the non-dimensional parameters shown. In the above, u_0 refers to any deflection of the body and $u_0/L\tau$ requires this to be in the same ratio as the thickness. The unsteady term Ut_0/L above defines the reference time t_0 for unsteady flow phenomena, and enters through the boundary conditions on the displacement. Eq. (2.8) can be rewritten in the form,

$$\frac{p}{\rho_\infty U^2 \tau^2} = \frac{1}{\gamma (M_\infty \tau)^2} + \Pi \left(x/L ; M_\infty \tau, \gamma, \frac{u_0}{L\tau}, \frac{Ut_0}{L} \right) \qquad (2.9)$$

From the above it is seen that the non-dimensional parameters required for similarity of hypersonic flows are,

$$M_\infty \tau, \quad \gamma, \quad \bar{\delta}, \quad \frac{u_0}{L\tau}, \quad \frac{Ut_0}{L} \qquad (2.10)$$

where $\bar{\bar{\delta}}$ represents the body thickness distribution of the family of bodies with different τ , and insures that they be affine. The above are applicable for M_∞ as low as 2.5.

At very high Mach numbers such that $M_\infty \tau \gg 1$ even though $\tau < 1$, the function Π becomes independent of $M_\infty \tau$ and approaches a limit. Also, the $1/\gamma(M_\infty \tau)^2$ term becomes small in comparison with Π and hence can be neglected. The $M_\infty \tau$ condition then drops out of Eq. (2.10) leaving only

$$\gamma, \quad \bar{\bar{\delta}}, \quad \frac{u_\circ}{L\tau}, \quad \frac{Ut_\circ}{L} \tag{2.11}$$

as the required similarity when $M_\infty \tau \gg 1$. The above is a more relaxed form of the Mach Number Independence Principle, Eq. (2.5), for no viscous effects, since now the thickness ratio τ need not be simulated, only its distribution $\bar{\bar{\delta}}$. The presence of real gas effects would result mainly in a somewhat lower value of γ here, but would probably not affect the inviscid pressure distribution markedly.

At hypersonic speeds, the shock wave about these slender bodies comes close to the surface, and causes interaction with a relatively thick viscous boundary layer. Significant changes in the pressure distribution may occur as a result. This viscous boundary layer, which is ordinarily neglected in determining the aerodynamic pressure distribution, must now be considered for these slender bodies. It brings in additional Reynolds number effects into the simple inviscid similarities of Eqs. (2.10) and (2.11).

This viscous interaction problem is considered by Hayes and Probstein in Ref. 2. The flow field outside the boundary layer on a slender body is considered to be the same as an inviscid flow field about the same body increased in its dimensions by the boundary layer displacement thickness. It is important then that the total thickness distribution including the displacement thickness be affinely related. This requires that the ratio of boundary layer displacement thickness δ^* to body thickness τL be maintained the same, thus introducing the additional similarity parameter, $\delta^*/\tau L$, to those of Eqs. (2.10) and (2.11). An analysis of the hypersonic boundary layer in Ref. 2 reveals that the parameter $\delta^*/\tau L$ can be replaced by

$$\underline{\chi} = \frac{1}{\tau\sqrt{\frac{\rho_w U L}{\mu_w}}} \qquad (2.12)$$

provided that P_r is the same, and that the non-dimensional temperature distribution T_w/T_s at the wall surface of the body be maintained the same on both model and prototype. In the above, ρ_w and μ_w refer to some point at the wall surface. Alternatively, the parameter $\underline{\chi}$ can be combined with the hypersonic similarity parameter $M_\infty \tau$ of Eq. (2.10) which after some manipulation gives the alternate parameter,* which after some manipulation gives the alternate parameter,

$$\overline{\chi} = \frac{M_\infty^3 \sqrt{C}}{\sqrt{Re_\infty}} \qquad (2.13)$$

---

*It can be shown that $\rho_w \propto \tau^2 \rho_\infty$ and that $T_w \propto M_\infty^2 T_\infty$. Also $\sqrt{C} \propto M_\infty^{s-1}$ where s is the exponent in the approximation $\mu \propto T^s$.

where

$$C = \frac{\mu_w T_\infty}{\mu_\infty T_w}$$

Adding these terms to Eq. (2.10), the pressure distribution similarity for a family of affine bodies in hypersonic flow, including the viscous interaction effects, requires the following parameters for low and moderate $M_\infty \tau$'s ,

$$M_\infty \tau, \ \gamma, \ \bar{\bar{\delta}}, \ \frac{u_o}{L\tau}, \ \frac{Ut_o}{L}, \ \frac{M_\infty^3 \sqrt{C}}{\sqrt{Re_\infty}}, \ \frac{T_w}{T_s}, \ P_r \qquad (2.14)$$

For very high Mach numbers where $M_\infty \tau \gg 1$, the parameters become,

$$\gamma, \ \bar{\bar{\delta}}, \ \frac{u_o}{L\tau}, \ \frac{Ut_o}{L}, \ \frac{1}{\tau\sqrt{\frac{\rho_w UL}{\mu_w}}}, \ \frac{T_w}{T_s}, \ P_r \qquad (2.15)$$

It is interesting to note that the above is a more relaxed version of the general Mach Number Independence Principle, Eq. (2.5), since Re_s now appears in combination with τ rather than separately.*

In the boundary layer theory used to obtain the similarity parameters of Eq. (2.14) and (2.15), it was assumed that the boundary layer is a perfect gas of constant γ , but that the viscosity μ may be variable. To account

*The fifth parameter of Eq. (2.15) as well as the sixth of Eq. (2.14) can be written alternatively as $1/\tau^2\sqrt{\frac{\rho_\infty UL}{\mu_s}}$.

more accurately for real gas effects, it is necessary to use the same gas and to maintain at least identical temperatures within the boundary layers of both model and prototype. This is achieved by additionally maintaining T_s the same, which from Eq. (2.4) implies U to be the same (for same gas). For the low and moderate $M_\infty \gamma$ case, the similarity parameters of Eq. (2.14) then increase to

$$M_\infty \gamma, \ \bar{\bar{\delta}}, \ \frac{u_o}{L\gamma}, \ \frac{t_o}{L}, \ U, \ \gamma^4 \rho_\infty L, \ \frac{T_w}{T_s}, \ \text{same gas} \qquad (2.16)$$

The same relations hold without the $M_\infty \gamma$ term when $M_\infty \gamma \gg 1$. These constitute Similarity Cases (B) of Ref. 2.

For even closer representation of the real gas effects in the boundary layer, it is also proposed in Ref. 2 to maintain identical pressures as well as identical temperatures over both model and prototype thereby assuring that the gas is in the same state. This may be achieved by maintaining the same $\rho_\infty U^2 \gamma^2$ as well as the same T_s (hence U) on both model and prototype (see Eq. 2.9). Introducing these into the low and moderate $M_\infty \gamma$ case, the similarity parameters of Eq. (2.16) increase to

$$M_\infty \gamma, \ \bar{\bar{\delta}}, \ \frac{u_o}{L\gamma}, \ \frac{t_o}{L}, \ U, \ \gamma^2 \rho_\infty, \ \gamma^2 L, \ \frac{T_w}{T_s}, \ \text{same gas} \qquad (2.17)$$

The same relations without the $M_\infty \gamma$ term hold for the $M_\infty \gamma \gg 1$ case. These constitute Similarity Cases (A) of Ref. 2.

It is probably sufficient for many cases of aerodynamic pressure distribution similarity to utilize Eqs. (2.14) and (2.15). It is to be noted that for small values of the parameter $\bar{\chi}$ of Eq. (2.13), viscous interaction effects are weak and can be neglected thus dropping out the $\bar{\chi}$ and associated temperature effects and leading back to the inviscid pressure distribution similarity of Eqs. (2.10) and (2.11).

c) Blunt Nosed Slender Bodies

The leading edges of slender bodies are generally blunted to reduce the high heat transfer rates at supersonic and hypersonic speeds. It has been found experimentally that even slight blunting may induce significant inviscid pressure distributions over a body surface at hypersonic speeds, (Ref. 7). On the basis of hypersonic small perturbation theory, Cheng in Ref. 8 derives the following additional similarity parameter to account for these blunt nose effects on pressure distributions,

$$\begin{cases} M_\infty^3 k \frac{d}{L} & \text{for plane surfaces} \\ M_\infty^2 k^{1/2} \frac{d}{L} & \text{for bodies of revolution} \end{cases} \qquad (2.18)$$

In the above, d is some typical dimension of the blunt nose (the diameter for cylinders and spheres) and k is the nose drag coefficient, which varies between 1, 4/3, 2 for spherical, cylindrical, and flat noses, respectively, in hypersonic flows. Since k is not particularly sensitive to the geometry and since presumably both model and prototype will

have the same general form of blunting, the dependence on k in the similarity parameter of Eq. (2.18) can be dropped.

The similarity parameter of Eq. (2.18) has correlated data for $5 < M_\infty < 20$ quite reasonably for the p/p_∞ on a flat plate afterbody for different combinations of M_∞ and d, (Ref. 8). The similarity parameter of Eq. (2.18) also occurs in the "blast-wave solution" for blunt nosed bodies (Ref. 9).

The basic similarity parameters for aerodynamic pressure distribution on blunt-nosed slender bodies in hypersonic flow can be obtained by adding the bluntness parameter, Eq. (2.18), to those of Eq. (2.14). For lifting surfaces, these become,

$$M_\infty \gamma \,,\quad \gamma \,,\quad \bar{\delta} \,,\quad \frac{u_o}{L\gamma} \,,\quad \frac{Ut_o}{L}$$

$$M_\infty^3 \sqrt{C}/\sqrt{Re_\infty} \,,\quad \frac{T_w}{T_s} \,,\quad P_r \,,\quad M_\infty^3 k \frac{d}{L} \qquad (2.19)$$

The above presumably account for both viscous interaction and blunting effects. Again, for $M_\infty \gamma \gg 1$, the dependence on $M_\infty \gamma$ can be neglected. Also the above can be made more precise by using the conditions of Eqs. (2.16) and (2.17). In maintaining similarity, the blunting effects are controlled by the independent quantity d which can be varied at one's disposal. It is to be noted that at small values of the parameter $M_\infty^3 k \frac{d}{L}$, the blunting effects become small and can be neglected.

d) Free Molecule Flow Regime

At extremely high altitudes the air may be rarefied to the extent where continuum concepts no longer

apply. The parameter distinguishing flow regions is the Knudsen number $K_n = \lambda/L$, where λ is the molecular mean free path and L a characteristic body dimension. In terms of free stream flow paramters,

$$K_n \propto \frac{M_\infty}{Re_\infty} \tag{2.20}$$

Free molecule flow is considered to be established when $M_\infty/Re_\infty > 10$, according to the criterion established by Tsien, (Ref. 10). Reference 11 indicates that free molecule flow in the case of a cylinder can also be characterized by $K_n > 2$. Generally, for satellite velocity vehicles, the free molecule regime can be considered as starting above about 90 miles altitude.

Utilizing concepts from the kinetic theory of gases, the pressure distribution about a body in free molecule flow is, (Ref. 12),

$$\frac{p}{\frac{1}{2}\rho_\infty U^2/S^2} = \left[\frac{(2-f)}{\sqrt{\pi}} S \sin\beta + \frac{f}{2}\sqrt{\frac{T_w}{T_\infty}}\right] e^{-S^2\sin^2\beta} + \left[(2-f)\left(\frac{1}{2} + S^2\sin^2\beta\right) + \frac{f}{2}\sqrt{\pi}\sqrt{\frac{T_w}{T_\infty}}\, S\sin\beta\right]\left[1+\operatorname{erf}(S\sin\beta)\right] \tag{2.21}$$

where f is the fraction of molecules that are diffusely reflected from the surface, S is the molecular speed ratio $U/\sqrt{2RT_\infty}$, T_∞ is the temperature of the incident stream and β is the angle between U and an element of surface (the local angle of attack). The wall temperature ratio T_w/T_∞ must be determined from energy transfer considerations at

the surface and will be discussed later. The molecular speed ratio S acts like a Mach number and is in fact related to the Mach number through $S = M_\infty \sqrt{\gamma/2}$.

The resulting similarity parameters for pressure distribution about a body in free molecule flow are seen to be

$$S \sin\beta \quad , \frac{T_w}{T_\infty} \quad , \quad f \quad , \quad \frac{U t_o}{L} \tag{2.22}$$

The parameter f depends primarily on the surface material and condition and generally varies between .8 and 1.0. The unsteady condition Ut_o/L enters through the motion of the boundary, and defines the reference time t_o. The Reynolds number plays no role other than that of serving to define the flow regime according to the Tsien criterion, $M_\infty/Re_\infty > 10$.

In high speed free molecule flow around the nose of a blunt body ($S >> 1$, $\sin\beta$ of order of 1,) Eq. (2.21) can be reduced to

$$\frac{p}{p_s} \approx \sin^2\beta \tag{2.23}$$

where

$$p_s = (2-f)\rho_\infty U^2$$

Thus for high speed free molecule flow the pressure distribution about a blunt body tends to become independent of S (or M_∞), T_w/T_∞ and f. One need only simulate here the same geometry (β) as in the continuum hypersonic flow case.*

*Note that slightly differing values of f can readily be accounted for in p_s.

This independence of S at large values of S is also shown to exist theoretically and experimentally for the lift and drag coefficients about various bodies in Refs. 13 and 14.

For affinely related slender bodies of differing thickness ratios τ, the form of Eqs. (2.10) and (2.22) leads to the similarity parameters

$$S\tau, \quad \bar{\bar{\delta}}, \quad \frac{u_0}{L\tau}, \quad \frac{T_w}{T_\infty}, \quad f, \quad \frac{Ut_0}{L} \tag{2.24}$$

At very high molecular speed ratios S such that $S\tau \gg 1$ even though $\tau < 1$, Eq. (2.21) reduces to

$$\frac{p}{\rho_\infty U^2 \tau^{2(2-f)}} \approx \left[\left(\frac{u_0}{\tau L}\right)\left(\frac{L}{Ut_0}\right)\frac{\partial \bar{w}}{\partial \bar{t}} + \frac{\partial}{\partial \bar{x}}\left(\frac{\bar{\bar{\delta}}}{2} + \frac{u_0}{L\tau}\bar{w}\right)\right]^2 \tag{2.25}$$

Leaving only the parameters

$$\bar{\bar{\delta}}, \quad \frac{u_0}{L\tau}, \quad \frac{Ut_0}{L} \tag{2.26}$$

as the required similarity for $S\tau \gg 1$. In Eq. (2.25), w represents the deflection of the midplane.

The above behavior at high S for blunt bodies and at high $S\tau$ for slender bodies is exactly analogous to that of continuum hypersonic flow as discussed in Section 2.2. Thus the Mach Number Independence Principle appears operative in the free molecule flow regime as well as in the continuum hypersonic region.

2.3 Aerodynamic Heat Transfer Similarity

The aerodynamic flow over a cool body in high speed flow causes an aerodynamic heat input rate q_A to flow into the body. This q_A, resulting from the viscous and boundary layer effects, causes a subsequent rise in the body temperature. As is shown later by an examination of the gas body boundary condition in Section 3.1, similarity of the subsequent body temperatures requires simulation of the Biot number parameter,

$$\frac{q_A L}{K_o T_o} \tag{2.27}$$

where K_o represents the reference heat conduction coefficient of the body, T_o represents a reference temperature (can be taken equal to T_s if desired), and q_A is the aerodynamic heat transfer rate over the body surface. Since $q_A = k\,(\partial T/\partial n)_{GAS}$ at the surface, the above condition of Eq. (2.27) can be reduced to a condition of

$$\frac{k_s}{K_o} \tag{2.28}$$

provided the non-dimensional temperature distribution $\bar{T}$ is the same at corresponding points in the flow field close to the body (boundary layer). This will occur if the complete similarity conditions of Eq. (2.2) for supersonic or Eq. (2.5) for hypersonic flow are fulfilled.

To search for less restrictive similarity conditions pertaining specifically to the heating of the body, various expressions for the aerodynamic heat transfer rate q_A are examined. These can then be placed into Eq. (2.27) to

obtain specific combined parameters which may be less restrictive than the parameters of Eq. (2.2) or (2.5) plus Eq. (2.28).

a) Stagnation Point

The most severe heating rates of a hypersonic vehicle will probably be experienced at the stagnation point of the body or wing leading edge. The high stagnation temperatures behind the shock wave of a blunt nosed surface in hypersonic flow will dissociate the air which may subsequently recombine in the gas phase of the flow or at the body surface if the surface is catalytic. This recombination process may appreciably add to the heat transferred by normal molecular conduction under certain circumstances.

The boundary layer at the stagnation point will most likely be laminar. The stagnation point heat transfer rate for such a dissociating gas in hypersonic flow is given by Fay and Riddell in Ref. 15 as

$$q_A = \frac{.76\sqrt{\rho_s \mu_s}}{\sqrt{R}\ Pr_s^{.6}} (h_s - h_w)\left(\frac{2\rho_s}{\rho_s}\right)^{\frac{1}{4}}\left(\frac{\rho_w \mu_w}{\rho_s \mu_s}\right)^{.1}\left[1 + (L_e^n - 1)\frac{h_D}{h_s}\right] \qquad (2.29)$$

where R is the nose radius of curvature, h_D is the amount of the stagnation enthalpy h_s outside the boundary layer involved in dissociation and L_e is the Lewis number $\rho D C_p/k$. The Lewis number for air does not vary appreciably and is in the range from 1.0 to 1.5.

The effects of dissociation are accounted for principally by the bracketed term of Eq. (2.29). If the dissociation species recombine rapidly in the gas phase (equilibrium flow) n = .52, and if recombination proceeds

slowly (frozen flow) n = .63. If the flow is frozen, the dissociated air may diffuse through the boundary layer and recombine at the body surface if the surface is catalytic. This latter frozen-catalytic wall case produces almost the same heat transfer as does the equilibrium flow case. Only in the frozen-non-catalytic wall case is there any appreciable reduction in q_A . In such an event, consideration of such effects as the recombination rates in the gas and at the wall is necessary for detailed simulation of the heat transfer process. These effects are described further in Ref. 15 and 16.

Making use of the hypersonic approximations for the stagnation point quantities, Eq. (2.4), and placing q_A of Eq. (2.29) into the heat conduction similarity parameter $q_A L / K_0 T_0$ will result in

$$\frac{q_A L}{K_0 T_0} = .76 \frac{k_s}{K_0} \sqrt{\frac{\rho_\infty U L}{\mu_s}}\, P_{r_s}^{.4}\, \frac{h_s}{c_{p_s} T_0} \left\{ \left(\frac{\gamma+3}{\gamma+1}\right)^{\frac{1}{2}} \left(\frac{\gamma}{\gamma-1}\right)^{\frac{1}{4}} \left(\frac{\rho_w \mu_w}{\rho_s \mu_s}\right)^{.1} \right\} \left[1 + (Le^n - 1) \frac{h_D}{h_s} \right] \left(1 - \frac{T_w}{T_s}\right) \quad (2.30)$$

where L is now a characteristic length pertaining to the nose region, and h_s is the stagnation enthalpy of the flow ($h_s \approx U^2/2$ if it results purely from velocity conversion into enthalpy). From the above the similarity parameters for aerodynamic heating become

$$\frac{k_s}{K_0} \sqrt{Re_s}\, P_{r_s}^{.4}\, \frac{h_s}{c_{p_s} T_0} \left\{ \left(\frac{\gamma+3}{\gamma+1}\right)^{\frac{1}{2}} \left(\frac{\gamma}{\gamma-1}\right)^{\frac{1}{4}} \left(\frac{\rho_w \mu_w}{\rho_s \mu_s}\right)^{.1} \right\} \left[1 + (Le^n - 1) \frac{h_D}{h_s} \right] , \quad \frac{T_w}{T_s} \qquad (2.31)$$

The first parameter is seen to be a combined grouping of the individual parameters for similarity, that is Eq. (2.5) plus Eq. (2.28), and as such, considerable adjustment can be made of them. The brace $\{\quad\}$ quantity is a weakly varying function of temperature and for air does not vary more than a few percent over the range to be encountered in re-entry heating problems. The second parameter requires that similar wall temperatures be maintained. It is to be noticed that for initially cool bodies in high stagnation temperature air streams where $T_w \ll T_s$, the h_w term may be neglected in comparison with h_s in Eq. (2.29). This then causes the second parameter, T_w/T_s, to drop out, leaving additional freedom in the choice of T_o for the first parameter (provided both model and prototype operate in the $T_w \ll T_s$ region).

For engineering purposes the following simple relation has been suggested in Ref. 17 for stagnation point heating in a hypersonic, highly cooled boundary layer ($T_w \ll T_s$), in equilibrium, laminar flow,

$$q_A = \frac{C_1}{\sqrt{R}} \sqrt{\rho_\infty}\, U^3 \tag{2.32}$$

where C_1 is some constant depending on the gas. This is obtainable from Eq. (2.29) by making a number of simplifying assumptions and seems to give reasonable estimates. (This expression also applies for frozen flow provided the surface is highly catalytic.) Placing this into the heat conduction similarity parameter $q_A L/K_o T_o$ results in the single similarity parameter for aerodynamic heating,

$$\frac{C_1\sqrt{\rho_\infty L}\,U^3}{K_0 T_0} \text{ or equivalently } C_1 \frac{k_s}{K_0}\sqrt{Re_s}\,Pr_s \frac{U^2}{c_{p_s} T_0}\sqrt{\frac{U}{\mu_s}} \qquad (2.33)$$

The second form of this is seen to be very similar to the more precise term of Eq. (2.31) with its brace { } and bracket [ ] terms removed, if the assumptions that $\mu_s \propto \sqrt{T_s}$ and $h_s \approx U^2/2$ are made. It is considerably simpler to use Eq. (2.33) for rough effects of similarity.

It has been shown in Ref. 18 that the heat transfer distribution $q_A/(q_A)_{STAG}$ in the vicinity of the stagnation point for laminar flow is relatively insensitive to variations in Mach number and Reynolds number, but rather depends mainly on the geometry. Thus for engineering purposes, simulation of the laminar heat transfer rate around a blunt body up to angles of about 80° from the stagnation point is achieved if the same geometry is maintained. This however depends on the flow being maintained laminar over this extent. The question of whether transition to turbulent flow will occur in this extent of 80° is intimately tied in with the Reynolds number of the flow. There seems to be some evidence that for many flight missions of the prototype, laminar flow will prevail because of the low densities of the higher atmosphere and the highly cooled walls. If this cannot be assured, it seems necessary to either simulate the Reynolds number individually for both model and prototype as well as some other quantities such as roughness, or else attempt to artificially induce transition by trip wires on the model.

b) Regions Away from Stagnation Point

On flat plate-like surfaces and at regions away from the stagnation point where pressure gradient effects

are insignificant, the following flat plate expressions for the heating rate q_A are often used

$$q_A = .332 (P_r)^{1/3} \sqrt{Re} \frac{k}{x} \frac{(h_r - h_w)}{c_p} \qquad \text{(laminar)} \qquad (2.34a)$$

$$q_A = .030 (P_r)^{1/3} (Re)^{.8} \frac{k}{x} \frac{(h_r - h_w)}{c_p} \qquad \text{(turbulent)} \qquad (2.34b)$$

where h_r is the recovery enthalpy ($h_r = h_s + r U^2/2$). These expressions have successfully correlated data for un-dissociated flow at high Mach numbers utilizing local values of the gas properties just outside the boundary layer. They are also applicable to the region around a blunt body aft of the stagnation point provided the pressure gradient does not vary too rapidly,(Ref. 19).

Making use of the hypersonic approximations and placing the above heating rates into the heat conduction similarity parameter $q_A L / K_0 T_0$ results in the parameters

$$\frac{k}{K_0} \sqrt{Re} (P_r)^{1/3} \frac{h_r}{c_p T_0} \quad , \quad \frac{T_w}{T_s} \qquad \text{(laminar)} \qquad (2.35a)$$

$$\frac{k}{K_0} (Re)^{.8} (P_r)^{1/3} \frac{h_r}{c_p T_0} \quad , \quad \frac{T_w}{T_s} \qquad \text{(turbulent)} \qquad (2.35b)$$

The above combined similarity parameters are quite similar in form to those derived for the laminar stagnation point heating rate, Eq. (2.31). Again, for highly cooled walls,

the second parameter T_w/T_s can be neglected in the similarity. It is to be noted that a small conflict will result if the above combined parameters are attempted to simulate simultaneously both the laminar and turbulent regions of flow because of the different powers of R_e . However the discrepancy is not great and some inaccuracy could probably be tolerated without having to resort to matching R_e , k/K_0 , and P_r separately. (Of more importance would be insuring that transition occured at the same point on model and prototype.)

c) Sharp-Nosed Slender Bodies

For a family of affinely related slender bodies of thickness ratio τ , Hayes and Probstein in Ref. 2 have shown through an analysis of the hypersonic laminar boundary layer that the laminar heating rate q_A can be expressed as,

$$q_A = \frac{\rho_\infty U^3 \tau}{\sqrt{\frac{\rho_\infty UL}{\mu_s}}} \Lambda \left(x/c;\ M_\infty \tau,\ \frac{T_w}{T_s},\ \gamma,\ P_r,\ \frac{u_0}{L\tau},\ \frac{Ut_0}{L} \right) \tag{2.36}$$

where Λ is a function of the parameters shown, and the stagnation enthalpy h_s has been taken as $h_s \approx U^2/2$. Placing the above into the heat conduction similarity parameter $q_A L/K_0 T_0$ results in the combined parameters,

$$\frac{h_s}{K_0}\sqrt{\frac{\rho_\infty UL}{\mu_s}}\ P_{r_s}\ \tau \frac{U^2}{c_{p_s} T_0},\ \frac{T_w}{T_s},\ M_\infty \tau,\ \gamma, \tag{2.37}$$

$$P_r,\ \bar{\delta},\ \frac{u_0}{L\tau},\ \frac{Ut_0}{L}$$

It is seen that the first parameter is a more relaxed version of the previous flat plate parameter, Eq. (2.35a), since here τ also appears in the combination. (The difference in the P_r power is not significant since P_r is required to be maintained separately anyway in Eq. 2.37). The second wall temperature parameters (T_w/T_s) are identical, and the remaining parameters of Eq. (2.37) are already required to insure that aerodynamic pressure similarity is being maintained over these slender bodies.

As mentioned in Section 2.2b, viscous interaction between the boundary layer and the flow field may play a significant role at these hypersonic speeds. To maintain the proper viscous interaction, one would need to add, as in the pressure distribution case, the interaction parameter,

$$\bar{\chi} = \frac{M_\infty^3 \sqrt{C}}{\sqrt{Re_\infty}} \tag{2.38}$$

to the parameters given by Eq. (2.37). For very high Mach numbers where $M_\infty \tau \gg 1$, the viscous interaction parameter of Eq. (2.38) is replaced by

$$\frac{1}{\tau^2 \sqrt{\frac{\rho_\infty U L}{\mu_s}}} \tag{2.39}$$

and the $M_\infty \tau$ parameter drops out of the grouping given by Eq. (2.37).

For heat transfer effects generally, the real gas effects are expected to play a larger role than for the pressure distribution effects. It would then probably be wise to see that at least identical temperatures are

maintained on the model and prototype. For this case, the parameters become those of Eq. (2.16) plus the combined parameter,

$$\frac{k_s}{K_0}\sqrt{\frac{\rho_\infty U L}{\mu_s}}\,P_{r_s}\,\gamma\,\frac{U^2}{c_{p_s}T_0} \tag{2.40}$$

If further, the same pressures as well as the same temperatures are to be maintained in order to insure the same equation of state, then similarity would require the parameters of Eq. (2.17) plus Eq. (2.40). Even then, it still might be necessary to consider recombination effects for complete similarity.

To account for the presence of blunt nosed slender bodies, the parameters of Eq. (2.18), $M_\infty^3 k \frac{d}{L}$ or $M_\infty^2 k^{1/2}\frac{d}{L}$, should be added to those already existing.

d) Free Molecule Flow Regime

Utilizing concepts from the kinetic theory of gases, the heat transfer rate in free molecule flow can be determined analogously to the pressure distribution. Following Ref. 20 this heat transfer can be expressed as,

$$q_A = \frac{a_e \rho_\infty U^3}{4\sqrt{\pi}\,S^3}\left\{\left[S^2+\frac{\gamma}{\gamma-1}-\frac{\gamma+1}{2(\gamma-1)}\frac{T_w}{T_\infty}\right]\left(e^{-S^2\sin^2\beta}+\sqrt{\pi}\,S\sin\beta\left[1+\operatorname{erf}(S\sin\beta)\right]\right)-\frac{1}{2}e^{-S^2\sin^2\beta}\right\} \tag{2.41}$$

where as before, S is the molecular speed ratio, γ is the specific heat ratio and a_e is an accomodation coefficient depending on the surface and is usually in the neighborhood of unity.

Placing the above into the heat conduction similarity parameter $q_A L/K_0 T_0$ results in the following general similarity parameters,

$$\frac{a_e \rho_\infty U^3 L}{S^3 K_0 T_0} \quad , \quad S \sin\beta \quad , \quad \frac{T_w}{T_\infty} \quad , \gamma, \; S \; , \; \frac{U t_0}{L} \tag{2.42}$$

The first parameter is the basic heat conduction requirement. It is interesting to note that it can be rearranged to give,

$$a_e \left(\frac{\rho_\infty U L}{\mu_\infty}\right) \frac{Pr_\infty}{S^3} \frac{k_\infty}{K_0} \frac{U^2}{c_{p_\infty} T_0} \tag{2.43}$$

thus resembling strongly the hypersonic continuum parameters of Eqs. (2.31), (2.35), and (2.37). Note that since S is required similar separately, it can be dropped from this first parameter. The second and third parameters of Eq. (2.42) are already required for simulation of the pressure distribution, (see Eq. 2.22), while the γ requirement is a relatively weak one mainly describing whether a monatomic or diatomic gas is present. The final requirement is that the speed ratio S be maintained separately as well as in combination with $S \sin\beta$.

In high speed free molecule flow around the nose of a cool blunt body ($S \gg 1$, $\sin\beta$ of order 1 , $T_w/T_\infty \ll S^2/3$), Eq. (2.41) can be reduced to

$$q_A \simeq \frac{a_e}{2} \rho_\infty U^3 \sin\beta \tag{2.44}$$

which when placed into the heat conduction parameter $q_A L/K_0 T_0$ yields the single heating similarity requirement,

$$\frac{a_e \rho_\infty U^3 L}{K_0 T_0} \tag{2.45}$$

The $\sin\beta$ term has been dropped in the above, since we are considering bodies of similar geometry (β distribution) here. Thus, it is seen that the heating characteristics tend to become independent of S, T_w/T_∞ and γ for this high speed cool blunt body case.

For affinely related cool slender bodies of differing thickness ratios τ in moderately high speed flow ($S > 3$, $T_w/T_\infty \ll S^2/3$), Eq. (2.41) can be reduced to

$$q_A \approx \frac{a_e \rho_\infty U^3}{4\sqrt{\pi}\, S}\left\{ e^{-(S\sin\beta)^2} + \sqrt{\pi}\, S\sin\beta\left[1 + \operatorname{erf}(S\sin\beta)\right]\right\} \tag{2.46}$$

The form of Eq. (2.46) then leads to the similarity parameters

$$\frac{a_e \rho_\infty U^3 L\tau}{K_0 T_0}\ ,\ S\tau\ ,\ \bar{\bar{\delta}}\ ,\ \frac{u_0}{L\tau}\ ,\ \frac{Ut_0}{L} \tag{2.47}$$

where the first parameter now has the thickness ratio τ combined with it. The $S\tau$ is the familiar hypersonic similarity parameter encountered in dealing with pressure distributions, while the next two parameters insure similarity of thickness distribution (family), and subsequent deflections.

At very high molecular speed ratios S, such

that $S\gamma \gg 1$ even though $\gamma < 1$, Eq. (2.46) reduces to Eq. (2.44) which then leads to the dropping of the parameter $S\gamma$ from eq. (2.47) leaving only

$$\frac{a_e \rho_\infty U^3 L \gamma}{K_0 T_0} \quad , \quad \bar{\bar{\delta}} \quad , \quad \frac{u_0}{L\gamma} \quad , \quad \frac{U t_0}{L} \tag{2.48}$$

Thus the heating behavior parallels the pressure distribution behavior discussed in Section 2.2d, and also exhibits the characteristics of the Mach Number Independence Principle.

In dealing with heating in free molecule flow, the above discussed aerodynamic heating rates are only one of the inputs to the system. Since these are in general quite small, other heating inputs of comparable or even greater magnitudes must also be considered when dealing with heat transfer in free molecule flow. Three of these that assume major significance are the solar heating rate q_{SOL}, the earth heating rate q_{ear}, and the radiation output from the body wall itself, $\epsilon_w \sigma T_w^4$. These inputs and outputs bring in the additional heating rate parameters

$$\frac{q_{SOL} L}{K_0 T_0} \quad , \quad \frac{q_{ear} L}{K_0 T_0} \quad , \quad \frac{\epsilon_0 T_0^3 L}{K_0} \tag{2.49}$$

into the problem. In their simulation, the proper distribution of these over the surface of the body is, of course, required. Often times the above parameters may be of much greater importance than the free molecule flow aerodynamic heating parameters previously discussed.

3. HEAT CONDUCTION SIMILARITY

3.1 Non-ablating Body

The equations governing the distribution of heat within a body are

$$\frac{\partial}{\partial x}\left(K\frac{\partial T}{\partial x}\right) + \frac{\partial}{\partial y}\left(K\frac{\partial T}{\partial y}\right) + \frac{\partial}{\partial z}\left(K\frac{\partial T}{\partial z}\right) = \rho_B C_p \frac{\partial T}{\partial t} \qquad (3.1)$$

$$\left(K\frac{\partial T}{\partial z}\right)_B = q_A - \epsilon_w \sigma T_w^4 \qquad (3.2)$$

These equations are similar to the equations treated in Ref. 1 except that now the heat flux from the boundary layer is written as q_A in place of $\left(k\,\partial T/\partial y\right)_{AIR}$. Eq. (3.1) governs the conduction of heat within the body subject to the boundary condition of Eq. (3.2) which expresses the balance of heat flux at the heated surface. As in Ref. 1 an insulated wall boundary condition ($K\partial T/\partial n = 0$) will not introduce any additional parameters to the equations above.

Non-dimensionalizing by introducing the following quantities:

$$\bar{x} = \frac{x}{L}\ , \quad \bar{y} = \frac{y}{L}\ , \quad \bar{z} = \frac{z}{L}$$

$$\bar{T} = \frac{T}{T_0}\ , \quad \bar{t} = \frac{t}{t_0} \qquad (3.3)$$

$$\bar{\bar{K}}_B = \frac{K}{K_0}\ , \quad \bar{\bar{C}}_{p_B} = \frac{C_p}{C_{p_0}}\ , \quad \bar{\bar{\epsilon}}_w = \frac{\epsilon_w}{\epsilon_0}$$

the above equations become

$$\frac{\partial}{\partial \bar{x}}\left(\bar{\bar{K}}_B \frac{\partial \bar{T}}{\partial \bar{x}}\right) + \frac{\partial}{\partial \bar{y}}\left(\bar{\bar{K}}_B \frac{\partial \bar{T}}{\partial \bar{y}}\right) + \frac{\partial}{\partial \bar{z}}\left(\bar{\bar{K}}_B \frac{\partial \bar{T}}{\partial \bar{z}}\right) = \left(\frac{L^2}{\pi_o t_o}\right) \bar{\bar{C}}_p \frac{\partial \bar{T}}{\partial \bar{t}} \quad (3.4)$$

$$\left(\bar{\bar{K}}_B \frac{\partial \bar{T}}{\partial \bar{z}}\right)_B = \frac{q_A L}{K_o T_o} - \left(\frac{\epsilon_o T_o^3 L}{K_o}\right) \bar{\bar{\epsilon}}_w \sigma \bar{T}_w^4 \quad (3.5)$$

where $\pi_o = K_o/\rho_B C_{p_o}$. The resulting non-dimensional parameters required for similarity in the temperature distribution $\bar{T}$ are

$$\frac{q_A L}{K_o T_o}, \frac{\epsilon_o T_o^3 L}{K_o}, \frac{\pi_o t_o}{L^2}, \bar{\bar{K}}_B, \bar{C}_{p_B}, \bar{\bar{\epsilon}}_w \quad (3.6)$$

The above parameters are similar to the parameters derived in Section 2.2 of Ref. 1, where the parameter $q_A L/K_o T_o$, which may be identified as the Biot number, corresponds to the k_∞/K_o parameter there. It should be noted however that replacing $q_A L/K_o T_o$ by k_∞/K_o requires the simulation of the temperature gradients in the boundary layer and these gradients generally depend on reproducing M_∞ and Re_∞ separately. The parameter $q_A L/K_o T_o$ also depends on M_∞ and Re_∞ through q_A , but as indicated in the preceding section M_∞ and Re_∞ appear in combined forms and in many cases (for sufficiently high M_∞) the dependence on M_∞ may be dropped. The actual form that the Biot number parameter $q_A L/K_o T_o$ does take on for various aerodynamic theories has been discussed in Section 2.3. It is to be noted that the heat flux q_A in the Biot number parameter may be of either aerodynamic or non-aerodynamic

origin.

The surface radiation parameter $\epsilon_0 T_0^3 L / K_0$, because of the resulting higher surface temperatures anticipated in hypersonic flight, is generally of considerable importance. If the same materials and temperatures are to be utilized reproduction of this parameter is possible only if the length scale ratio $L_P / L_M = 1$. Utilization of the same materials and temperatures is mandatory not only for simulation of the heat transfer problem (matching $\bar{\bar{K}}_B$ $\bar{\bar{C}}_{P_B}$, $\bar{\bar{\epsilon}}_W$) but also for structural deformation behavior as will be seen in the next section. The radiation parameter thus imposes a stringent restriction on the length ratio L_P / L_M and presents a basic obstacle.

Several possibilities exist in dealing with this obstacle. In one it may be possible to control the emmissivity by such means as coating the surface of the structure and thus not restricting the value of ϵ by a choice of materials. In this case, for the same materials and temperatures, the scale ratio as determined from $\epsilon_0 T_0^3 L / K_0$ will be

$$\frac{L_P}{L_M} = \frac{(\epsilon_0)_M}{(\epsilon_0)_P} \tag{3.7}$$

As $(\epsilon_0)_M$ can never be greater than 1, there is a limit to the scale ratio L_P / L_M that can be satisfied by this means, particularly if the prototype itself is operating at high emissivities $(\epsilon_0)_P$. In utilizing a surface coating to obtain the proper ϵ_0 , it should also be determined whether this coating affects the heat flux q_A .

A second means of alleviating the radiation obstacle occurs when considering flight near the equilibrium temperature. The equilibrium temperature is achieved after

a sufficiently long period of heating when the heat flux input balances the radiative heat loss. Transfer of heat by conduction is negligible (i.e., $(K\,\partial T/\partial z)_B = 0$ in Eq. 3.2), and the parameters of Eq. (3.6) are replaced by the following parameters

$$\frac{q_A}{\epsilon_0 T_0^4} \quad , \quad \bar{\bar{\epsilon}}_w \tag{3.8}$$

Therefore in this case no condition on the length scale appears directly. The parameter $q_A/\epsilon_0 T_0^4$ is particularly applicable to a hypersonic glide vehicle which by nature of its long flight time relies principally upon radiation as a cooling mechanism.

A further means of dealing with the radiation obstacle may be seen by rewriting Eq. (3.5) in the following non-dimensional form

$$\left(\bar{\bar{K}}_B \frac{\partial \bar{T}}{\partial \bar{z}}\right)_B = \left(q_A - \epsilon_w \sigma T_w^4\right)\frac{L}{K_0 T_0} = \frac{q_{NET} L}{K_0 T_0} \tag{3.9}$$

and thus directing attention to the net heat flux q_{NET} into the structure rather than treating q_A and the radiation loss $\epsilon_w \sigma T_w^4$ as two separate quantities. The parameters of Eq. (3.6) would then be replaced by

$$\frac{q_{NET} L}{K_0 T_0} \quad , \quad \frac{\pi_0 t_0}{L^2} \quad , \quad \bar{\bar{K}}_B \quad , \quad \bar{\bar{C}}_{p_B} \tag{3.10}$$

This procedure assumes, however, that q_A and T_w are known in advance (see further the discussion in Section 5.1e).

Having estimated the required q_{NET} for a particular test, it may be applied by such means as radiant heaters or a heated air stream. Use of radiant heaters may provide similarity in heat transfer and allow large scale ratios but will not account for any air loads. A heated air stream at a low M_∞ may provide similarity in heat transfer but may incorrectly scale the air load distribution. Tests of this second type have been conducted on multiweb wings by the NASA (see Ref. 21, for example).

Heat transfer similarity has been discussed above for a general body (Eqs. 3.1 and 3.2). Some less restrictive relationships can be obtained however when considering specific configurations such as thin skins and built up structures. The general ideas involved here are discussed in Ref. 1. For example, considering a thin plate of thickness δ which has a very small temperature variation through the plate in the $\bar{z}$ direction, the governing heat conduction equation becomes,

$$\frac{\partial}{\partial x}\left(K\delta\frac{\partial T}{\partial x}\right)+\frac{\partial}{\partial y}\left(K\delta\frac{\partial T}{\partial y}\right) = \rho_B C_p \delta\frac{\partial T}{\partial t} - q_A + \epsilon_w \sigma T_w^4 \qquad (3.11)$$

Non-dimensionalizing this, the appropriate similarity parameters are,

$$\frac{q_A L^2}{K_0 T_0 \delta_0}\ ,\ \frac{\epsilon_0 T_0^3 L^2}{K_0 \delta_0}\ ,\ \frac{\kappa_0 t_0}{L^2}\ ,\ \bar{\bar{K}}_B\ ,\ \bar{\bar{C}}_{p_B}\ ,\ \bar{\bar{\epsilon}}_W\ ,\ \bar{\bar{\delta}} \qquad (3.12)$$

The above are somewhat less restrictive than the parameters of Eq. (3.6) since they allow the thickness ratio $\tau = \delta_0/L$ of the plate to be varied in addition to the original quantities. However, both the prototype and model plates

must behave as thin plates with little temperature variation in the z direction.

Even further reduction in the similarity parameters can be achieved if it is assumed as well that the heat conduction in the x and y direction is also very small. In that case the parameters of Eq. (3.12) reduce still further to

$$\frac{q_A t_0}{\rho_B C_{p_0} \delta_0 T_0} \quad , \quad \frac{\epsilon_0 T_0^3 t_0}{\rho_B C_{p_0} \delta_0} \quad , \quad \bar{\bar{C}}_{p_B} \quad , \quad \bar{\bar{\epsilon}}_w \quad , \quad \bar{\bar{\delta}} \tag{3.13}$$

Such an assumption has been made for the heat conduction of thin two dimensional wings in Ref. 22.

3.2 Ablating Body

When the body temperature is sufficiently high the material may undergo a change of phase by either melting, accompanied with possible vaporization, or by sublimating. The process of absorbing heat by removal of the surface material is known as ablation and is of considerable current interest. It is likely to occur at the noses or leading edges of high speed vehicles where the aerodynamic heat transfer rates are apt to be very large.

The ablation process of a melting-vaporizing material near a stagnation point may be treated by studying the laminar boundary layer equations for a melt layer, which have the following forms (see Refs. 23, 24, and 25)

$$\frac{\partial(u r^j)}{\partial x} + \frac{\partial(v r^j)}{\partial z} = 0 \tag{3.14}$$

$$\frac{\partial p}{\partial x} = \frac{\partial}{\partial z}\left(\mu_L \frac{\partial u}{\partial z}\right) \tag{3.15}$$

$$\frac{\partial p}{\partial z} = 0 \tag{3.16}$$

$$\rho_L C_{p_L} \frac{\partial T}{\partial t} + \rho_L C_{p_L}\left[u \frac{\partial T}{\partial x} + v \frac{\partial T}{\partial z}\right] = \frac{\partial}{\partial z}\left(K_L \frac{\partial T}{\partial z}\right) + \frac{\partial}{\partial x}\left(K_L \frac{\partial T}{\partial x}\right) \tag{3.17}$$

where j = 0 for a two-dimensional flow and j = 1 for a body of revolution.

The inertia forces are small compared to the viscous forces and hence are usually neglected above ($Re_L \sim 1$). Also the viscous dissipation terms in the energy equation can be neglected. The accompanying governing equation for heat conduction in the body (Eq. 3.1) is

$$\rho_B C_{p_B} \frac{\partial T}{\partial t} = \frac{\partial}{\partial x}\left(K_B \frac{\partial T}{\partial x}\right) + \frac{\partial}{\partial z}\left(K_B \frac{\partial T}{\partial z}\right) \tag{3.18}$$

where the surface is a distance s from the initial pre-ablation position (see Fig. 3). The boundary conditions are

at z = h(t):

$$q_A - \eta \dot{m}_v (h_s - h_v) = -\left(K_L \frac{\partial T}{\partial z}\right)_L + \dot{m}_v L_v + \epsilon \sigma T^4$$

$$\tau_A = -\mu_L \frac{\partial u}{\partial z}, \quad p_L = p_A, \quad T = T_v \tag{3.19}$$

$$v = \frac{\partial h}{\partial t} + u \frac{\partial h}{\partial x} - \frac{\dot{m}_v}{\rho_L}$$

at z = s(t):

$$u = 0 \quad , \quad v = -\left(\frac{\rho_L - \rho_B}{\rho_B}\right)\dot{s} = -\frac{(\rho_L - \rho_B)}{\rho_L}\frac{\dot{m}_L}{\rho_L}$$

$$-K_L\left(\frac{\partial T}{\partial z}\right)_L = -K_B\left(\frac{\partial T}{\partial z}\right)_{B,\, z=s} + L_M \dot{m}_L \, , \quad T = T_M \tag{3.20}$$

where $\dot{m}_L$ and $\dot{m}_v$ are the mass rates of loss due to melting and vaporization, respectively, L_M and L_v are the heats of melting and vaporization respectively, η is an empirical factor associated with the heat blockage due to vapor injection, T_M and T_v are the melting and vaporization temperatures, respectively, h_s is the stagnation enthalpy, and $\dot{s} = \dot{m}_L/\rho_L$ is the ablation velocity. The aerodynamic heat transfer q_A, shear τ_A and pressure p_A are assumed known quantities for a non-ablating material, evaluated at the gas-melt interface, and were discussed in Section 2. (The shear stress τ_A is directly related to the heat transfer q_A through Reynold's analogy, $\tau_A / q_A = (P_{r_s})^{2/3} u / (h_s - h_i)$ where P_{r_s} is the stagnation Prandtl number of the gas.

Non-dimensionalizing by introducing the following,

$$\bar{u} = \frac{u}{V_0} \, , \quad \bar{v} = \frac{v}{V_0} \, , \quad \bar{p} = \frac{p}{p_0} \, , \quad \bar{T} = \frac{T}{T_0}$$

$$\bar{t} = \frac{t}{t_0} \, , \quad \bar{x} = \frac{x}{L} \, , \quad \bar{z} = \frac{z}{L} \, , \quad \bar{r} = \frac{r}{L} \tag{3.21}$$

$$\bar{\bar{K}}_L = \frac{K_L}{K_0} \, , \quad \bar{\bar{\rho}}_L = \frac{\rho_L}{\rho_0} \, , \quad \bar{\bar{C}}_{p_L} = \frac{C_{p_L}}{C_{p_0}} \, , \quad \bar{\bar{\mu}}_L = \frac{\mu_L}{\mu_0}$$

$$\bar{\bar{K}}_B = \frac{K_B}{K_0} \, , \quad \bar{\bar{\rho}}_B = \frac{\rho_B}{\rho_0} \, , \quad \bar{\bar{C}}_{p_B} = \frac{C_{p_B}}{C_{p_0}} \, , \quad \bar{\bar{\epsilon}}_w = \frac{\epsilon_w}{\epsilon_0}$$

equations (3.14) to (3.18) become

$$\frac{\partial(\bar{u}\bar{\rho}^{j})}{\partial\bar{x}} + \frac{\partial(\bar{v}\bar{\rho}^{j})}{\partial\bar{y}} = 0 \tag{3.22}$$

$$\left(\frac{\rho_0 L}{\mu_0 V_0}\right)\frac{\partial\bar{p}}{\partial\bar{x}} = \frac{\partial}{\partial\bar{z}}\left(\bar{\bar{\mu}}_L \frac{\partial\bar{u}}{\partial\bar{z}}\right) \tag{3.23}$$

$$\frac{\partial\bar{p}}{\partial\bar{z}} = 0 \tag{3.24}$$

$$\left(\frac{L^2}{\pi_0 t_0}\right)\bar{\rho}_L \bar{\bar{C}}_{p_L}\frac{\partial\bar{T}}{\partial\bar{t}} + \left(\frac{V_0 L}{\pi_0}\right)\bar{\rho}_L \bar{\bar{C}}_{p_L}\left[\bar{u}\frac{\partial\bar{T}}{\partial\bar{x}} + \bar{v}\frac{\partial\bar{T}}{\partial\bar{z}}\right] = \frac{\partial}{\partial\bar{x}}\left(\bar{\bar{K}}_L\frac{\partial\bar{T}}{\partial\bar{x}}\right) + \frac{\partial}{\partial\bar{z}}\left(\bar{\bar{K}}_L\frac{\partial\bar{T}}{\partial\bar{z}}\right) \tag{3.25}$$

$$\left(\frac{L^2}{\pi_0 t_0}\right)\bar{\bar{\rho}}_B \bar{\bar{C}}_{p_0}\frac{\partial\bar{T}}{\partial\bar{t}} = \frac{\partial}{\partial\bar{x}}\left(\bar{\bar{K}}_B\frac{\partial\bar{T}}{\partial\bar{x}}\right) + \frac{\partial}{\partial\bar{z}}\left(\bar{\bar{K}}_B\frac{\partial\bar{T}}{\partial\bar{z}}\right) \tag{3.26}$$

where $\pi_0 = K_0/\rho_0 C_{p_0}$ is the thermal diffusivity. Since stagnation point ablation is being considered, the characteristic length L in this case is appropriately the nose radius R. The reference quantities K_0, ρ_0, C_{p_0} refer to reference properties on the body.

The boundary conditions in non-dimensional form are

at $\bar{z} = \bar{h}(\bar{t})$:

$$\left(\frac{q_A L}{K_0 T_0}\right) - \left(\frac{\dot{m}_L C_{p_0} L}{K_0}\right)\left(\frac{\dot{m}_v}{\dot{m}_L}\right)\left[\frac{L_v + \eta(h_s - h_v)}{C_{p_0} T_0}\right] - \left(\frac{\epsilon_0 T_0^3 L}{K_0}\right)\bar{\epsilon}\,\sigma\,\bar{T}_i^4$$

$$= -\bar{\bar{K}}_L\left(\frac{\partial \bar{T}}{\partial \bar{z}}\right)_{L,\,\bar{z}=\bar{h}} \qquad (3.27)$$

$$\bar{\bar{\mu}}_L \frac{\partial \bar{u}}{\partial \bar{z}} = \frac{\tau_A L}{\mu_0 V_0}\,, \quad \bar{p} = \frac{p_A}{p_0}\,, \quad \bar{T} = \frac{T_v}{T_0}$$

$$\bar{v} = \left(\frac{L^2}{\kappa_0 t_0}\right)\left(\frac{\pi_0}{V_0 L}\right)\frac{\partial \bar{h}}{\partial \bar{t}} + \bar{u}\frac{\partial \bar{h}}{\partial \bar{x}} - \left(\frac{L^2}{\pi_0 t_0}\right)\left(\frac{\pi_0}{V_0 L}\right)\left(\frac{\dot{m}_v}{\dot{m}_L}\right)\frac{\partial \bar{s}}{\partial \bar{t}}$$

at $\bar{z}\ \bar{s}(\bar{t})$:

$$\bar{u} = 0\,, \quad \bar{T} = \frac{T_M}{T_0}\,, \quad \bar{\rho}_L \bar{v} = -\left(\frac{\dot{m}_L C_{p_L} L}{K_0}\right)\left(\frac{\pi_0}{V_0 L}\right)\left(\frac{\bar{\bar{\rho}}_L - \bar{\bar{\rho}}_B}{\bar{\bar{\rho}}_L}\right)$$

$$-\bar{\bar{K}}_L\left(\frac{\partial \bar{T}}{\partial \bar{z}}\right)_{L,\,\bar{z}=\bar{s}} = -\bar{\bar{K}}_B\left(\frac{\partial \bar{T}}{\partial \bar{z}}\right)_{B,\,\bar{z}=\bar{s}} + \left(\frac{\dot{m}_L C_{p_L} L}{K_0}\right)\left(\frac{L_M}{C_{p_0} T_0}\right) \qquad (3.28)$$

The important unknown non-dimensional quantities to be solved for from Eqs. (3.22) to (3.28) above, are the ablation rate, the fraction of melt vaporized, and the temperature distribution within the body

$$\frac{\dot{m}_L C_{p_0} L}{K_0}\,, \quad \frac{\dot{m}_v}{\dot{m}_L}\,, \quad \bar{T}_B \qquad (3.29)$$

The parameters on which these unknowns depend are

obtained from Eqs. (3.22) to (3.28) as follows,

$$\frac{q_A L}{K_0 T_0}\ ,\ \frac{\epsilon_0 T_0^3 L}{K_0}\ ,\ \frac{\pi_0 t_0}{L^2}\ ,\ \frac{T_M}{T_0}\ ,\ \frac{L_M}{C_{p_0} T_0}\ ,\ \frac{\gamma_A L}{\mu_0 V_0}$$

$$\frac{p_0 L}{\mu_0 V_0}\ ,\ \frac{V_0 L}{\pi_0}\ ,\ \frac{T_v}{T_0}\ ,\ \frac{L_v + \eta(h_s - h_v)}{C_{p_0} T_0}\ ,\ \frac{p_A}{p_0} \qquad (3.30)$$

$$\bar{\bar{K}}_B\ ,\ \bar{\bar{C}}_{p_B}\ ,\ \bar{\bar{\rho}}_B\ ,\ \bar{\bar{K}}_L\ ,\ \bar{\bar{C}}_{p_L}\ ,\ \bar{\bar{\rho}}_L\ ,\ \bar{\bar{\mu}}_L$$

The above are applied to high speed stagnation point flow by setting the reference pressure p_0 equal to the stagnation pressure, then substituting for p_A from Eq. (2.6) and for γ_A from Reynolds analogy

$$p_0 = p_s = \rho_\infty U^2$$

$$p_A = \rho_\infty U^2 \sin^2\beta \qquad (3.31)$$

$$\gamma_A = C_2 \frac{g_A (P_r)^{2/3}}{U} \frac{x}{R}$$

where C_2 is some numerical constant.

The similarity parameters of Eq. (3.30) finally become, after slight rearrangement,

$$\frac{g_A L}{K_0 T_0}\ ,\ \frac{\epsilon_0 T_0^3 L}{K_0}\ ,\ \frac{\pi_0 t_0}{L^2}\ ,\ \frac{T_M}{T_0}\ ,\ \frac{L_M}{C_{p_0} T_0}$$

$$\frac{(P_{r_s})^{2/3} K_0 T_0 L}{U \mu_0 \pi_0}\ ,\ \frac{\rho_\infty U^2 L^2}{\mu_0 \pi_0}\ ,\ \frac{V_0 L}{\pi_0}\ ,\ \frac{T_v}{T_0}\ ,\ \frac{L_v + \eta(h_s - h_v)}{C_{p_0} T_0}$$

$$\beta\ ,\ \bar{\bar{K}}_s\ ,\ \bar{\bar{C}}_{p_s}\ ,\ \bar{\bar{\rho}}_s\ ,\ \bar{\bar{K}}_L\ ,\ \bar{\bar{C}}_{p_L}\ ,\ \bar{\bar{\rho}}_L\ ,\ \bar{\bar{\mu}}_L \qquad (3.32)$$

The above are the main ablation similarity parameters. The first three parameters are the same as derived previously in Section 3.1 for the non-ablating body. The following five parameters refer to the melting ablation process. Taking them in order, the fourth parameter serves to define the reference temperature T_0 , the fifth gives a condition on the latent heat of melting, the sixth on the shear forces acting on the melted layer, the seventh on the pressure forces, and the eighth serves to define the reference velocity V_0 associated with the flow of the molten layer. The next two parameters refer to the vaporizing process and give conditions on the vaporizing temperature* and effective heat of vaporization respectively, and the eleventh is a condition on geometry. The remaining parameters require similarity in variation with temperature of the material properties both in the solid and the liquid range. As given in Eq. (3.32) the parameters apply to a combined melting and subsequent vaporization process. If only melting is present (as in metals or at early times before a sufficient vaporization temperature is achieved), the vaporization parameters drop out. If the ablation is a sublimation process, then the melting parameters drop out. Also, if all the melt is removed immediately as it is formed, the liquid layer does not enter the problem, and the 6th, 7th, and 8th parameters above which relate to the flow of this

*Note though that the vaporization temperature of some materials, such as glasses, may themselves be complex functions of other parameters of the problem, for example, pressure.

layer would not be present.

Reproduction of the parameters of Eq. (3.32) will simulate a detailed study of the ablation process. In particular, the non-dimensional quantities,

$$\frac{\dot{m}_L C_{p_0} L}{K_0} \quad , \quad \frac{\dot{m}_v}{\dot{m}_L} \quad , \quad \bar{T}_B \tag{3.33}$$

will be the same for both prototype and model at corresponding non-dimensional times $\bar{t}$. In many instances, the structural designer is not concerned with the details of the ablation process but rather is interested in simulating only the temperature distribution $\bar{T}$ within the body, and in knowing the rate of ablation $\dot{m}_L$. In this case, the net balance of heat flux at the surface z = s is of interest. With the use of Eqs. (3.19) and (3.20) this net heat balance, replacing Eq. (3.2), is

$$-\left(K_B \frac{\partial T}{\partial z}\right)_{B,\, z=s} = q_A - \dot{m}_L \left\{ L_M + \left(\frac{\dot{m}_v}{\dot{m}_L}\right)\left[L_v + \eta (h_s - h_v) \right] \right. \\ \left. + \left(K_L \frac{\partial T}{\partial z}\right)_{L,\, z=h} - \left(K_L \frac{\partial T}{\partial z}\right)_{L,\, z=s} - \epsilon_w \sigma T_v^4 \right. \tag{3.34}$$

Assuming steady-state ablating conditions are reached, it can be shown that (see Ref. 25, for example)

$$\left(K_L \frac{\partial T}{\partial z}\right)_{L,\, z=h} - \left(K_L \frac{\partial T}{\partial z}\right)_{L,\, z=s} \approx -.60\, \dot{m}_L C_{p_L} (T_v - T_m) \tag{3.35}$$

$$\left(K_B \frac{\partial T}{\partial z}\right)_{B,\, z=s} = - C_{p_B} \dot{m}_L (T_m - T_c) \tag{3.36}$$

Utilizing Eq. (3.35) and (3.36), the heat flux relation, Eq. (3.34), becomes in non-dimensional form,

$$\frac{\dot{m}_L C_{P_0} L}{K_0} = \frac{\left(\frac{q_A L}{K_0 T_0}\right)}{\left\{\frac{C_{P_\theta}(T_M - T_0) + L_M + .60\, C_{P_L}(T_v - T_M) + (\dot{m}_v/\dot{m}_L)[L_v + \eta(h_s - h_v)]}{C_{P_0} T_0 \left(1 - \frac{\epsilon_w \sigma T_v^4}{q_A}\right)}\right\}} \quad (3.37)$$

The above gives the non-dimensional melting rate for steady state ablation. It represents a combined grouping of the individual ablation parameters given in Eq. (3.32), and hence also gives some indication as to which are the more significant of these parameters. If a judicious guess for the unknown $\dot{m}_v/\dot{m}_L$ appearing in it can be made, the steady-state ablation rate is then known. Also, the rough temperature distribution within the body could be obtained from Eq. (3.36) as,

$$\bar{T}_M \quad \text{on the surface}$$

$$\text{slope} \quad \frac{d\bar{T}}{d\bar{z}} = -\frac{1}{\bar{K}_\theta}\left(\frac{\dot{m}_L C_{P_\theta} L}{K_0}\right)(\bar{T}_M - \bar{T}_c) \quad \text{at the surface} \quad (3.38)$$

$$\bar{T}_c \quad \text{in the interior}$$

In dimensional form, Eq. (3.37) is often written as

$$\dot{m}_L = \frac{q_A}{H_{eff}} \quad (3.39)$$

where H_{eff} is defined as the effective heat of ablation in units of BTU/ lb, and is given, for the case considered above, by

$$H_{eff} = \frac{C_{P_B}(T_M - T_c) + L_M + .60 C_{P_L}(T_v - T_M) + \left(\frac{\dot{m}_v}{\dot{m}_L}\right)\left[L_v + \eta(h_s - h_v)\right]}{1 - \frac{\epsilon_w \sigma T_v^4}{q_A}} \quad (3.40)$$

It is seen that radiation may increase H_{eff} considerably. Furthermore, if the radiation loss is neglibible ($\epsilon_w \sigma T_v^4 / q_A \approx 0$), H_{eff} becomes independent of the length scale L which appears through the term q_A. Efficient ablators generally operate with considerable vaporization present, and so the $(\dot{m}_v/\dot{m}_L)[\quad\quad]$ term generally predominates over the preceding terms. The above expression for H_{eff} is frequently used by structural designers to estimate roughly ablation shield requirements (see Ref. 26). However, it should be born in mind that Eqs. (3.37) and (3.40) represent steady-state ablation rates, and that $\dot{m}_v/\dot{m}_L$ is estimated. For a more accurate detailed simulation of the transient ablation process, the parameters of Eqs. (3.32) should be used.

4. STRESS AND DEFLECTION SIMILARITY

The high structural temperatures and air loads associated with flight at high Mach numbers may no longer justify the assumption of an elastic structure made in Ref. 1, and additional structural and material considerations are necessary. Structural deflections may extend into the plastic range in which case material yield and ultimate stresses and plastic stress-strain behavior must be considered. Furthermore, the assumption of small deflections may have to be removed and it may be necessary to scale the structural deflections in the same scale as the characteristic dimensions of the body. At high temperatures the creep and fatigue characteristics of a structure may have to be considered which introduce time, temperature level and stress level as additional parameters. For convenience, the stress and deflection problem is divided into two major categories, namely, short-time loading and long-time loading.

4.1 Short-Time Loading

a) General

This category is concerned with loads of sufficiently short duration such that the stress deformation behavior of the material is not influenced appreciably by the time under load, i.e., creep and fatigue effects are absent. The material behavior can then be described solely by means of stress-strain curves at the particular operating temperature. It should be noted that for very short duration loads (high strain rates), these curves tend to become additionally dependent on strain rate $\dot{\epsilon}$. The stress deflection behavior considered here will be at stress levels between the yield point and the ultimate stress. The parameters for the elastic range have been derived previously in Ref. 1.

In this regime nonrecoverable deformations may result which may alter the steady-state deflections of the wing, the internal structural geometry, and the wing profile. These deformations may subsequently alter the air load distribution acting on the structure. Plastic buckling may also occur in members subjected to compressive forces. Essentially then, this category is an extension of the elastic structure study of Ref. 1, Section 2.3, into the plastic range and the additional parameters which must be included relate to the short-time plastic stress-strain behavior of a material. The similarity parameters required for the same stress distribution are thus

$$\frac{\sigma_0}{E_0}\ , \qquad \text{shape of stress-strain curve,}\ \ \alpha_0 T_0,$$

$$\overline{T}_0\ ,\ \frac{u_0}{L}\ ,\ \frac{\rho_0 L^2}{\sigma_0 t_0^2}\ ,\ \frac{\rho_0 g L}{\sigma_0}\ ,\ \overline{\overline{E}}\ ,\ \overline{\overline{\lambda}}\ ,\ \nu \qquad (4.1)$$

The first three parameters above relate to static stress-strain behavior, the fourth to the body temperature distribution, the fifth to scaled structural deflections, the sixth to structural dynamic effects, and the seventh to gravitational forces. The last three are conditions on material properties which are automatically fulfilled if the same materials and temperatures are utilized. For convenience, the reference stress σ_0 may be taken as the yield stress of the material. Note that for an elastic body the condition on the shape of the stress-strain curve above is automatically met.

The simulation of the general shape of the stress-strain curve is a very difficult task for anything except the same material at the same temperature. An attempt at this can be made though, through the Ramberg-Osgood

approximation. It has been shown that for many metals at various temperatures and various soaking times the following Ramberg-Osgood expression is a reasonable approximation (Ref.27)

$$\epsilon = \frac{\sigma}{E}\left[1 + \frac{3}{7}\left(\frac{\sigma}{\sigma_{.7}}\right)^{n-1}\right] \qquad (4.2)$$

where $\sigma_{.7}$ is the stress corresponding to a secant modulus of .7E and n is the shape factor of the curve. Both E and $\sigma_{.7}$ are now functions of temperature T. Non-dimensionalizing, Eq. (4.2) becomes

$$\epsilon = \frac{\sigma_o}{E_o}\frac{\bar{\sigma}}{\bar{\bar{E}}}\left[1 + \frac{3}{7}\left(\frac{\sigma_o}{(\sigma_{.7})_o}\frac{\bar{\sigma}}{\bar{\bar{\sigma}}_{.7}}\right)^{n-1}\right] \qquad (4.3)$$

where $\bar{\sigma} = \frac{\sigma}{\sigma_o}$ and $\bar{\bar{\sigma}}_{.7} = \frac{\sigma_{.7}}{(\sigma_{.7})_o}$.

In the above, $(\sigma_{.7})_o$ is the $\sigma_{.7}$ at some reference temperature.

Thus the entire shape of the stress-strain curve is reasonably well reproduced if the following parameters are duplicated

$$\frac{\sigma_o}{E_o}\ ,\ \bar{\bar{E}}\ ,\ \frac{\sigma_o}{(\sigma_{.7})_o}\ ,\ \bar{\bar{\sigma}}_{.7}\ ,\ n\ ,\ \frac{\sigma_{ULT}}{\sigma_{.7}} \qquad (4.4)$$

The first and second conditions above were previously derived for a body in the elastic region; the remaining ones are now additional conditions for the plastic portion of the stress-strain curve. The parameter $\sigma_o/(\sigma_{.7})_o$ serves to define the reference stress level σ_o , while the $\bar{\bar{\sigma}}_{.7}$ condition requires the $\sigma_{.7}$ to have the same variation with temperature on model and prototype. The parameter $\sigma_{ULT}/\sigma_{.7}$

is introduced to account for the extent of the plastic region and may be dispensed with if both model and prototype operate below their ultimate strengths. With regard to the shape parameter n, for 4340 steel, stainless steel W and Inconel X, for example, $n > 10$ up to $1200^{\circ}F$ and $n \approx 10$ approximates many of the aircraft metal alloys at room and elevated temperatures. The shape parameter n, being approximately the same for many aircraft materials, may therefore be dispensed with. Under all the above conditions, the first two parameters of Eq. (4.1) may then be replaced by the following:

$$\frac{\sigma_o}{E_o} \quad , \quad \frac{\sigma_o}{(\sigma_{.7})_o} \quad , \quad \bar{\bar{\sigma}}_{.7} \tag{4.5}$$

where it has been assumed that all stresses are acting below the ultimate stress of the material. An additional condition is necessary relating to the normal stress boundary condition on the structure. At the surface of the body, the normal stress σ_n equals the sum of the aerodynamically applied pressure p_A and any additional non-aerodynamic loading p_F . This then introduces the additional non-dimensional parameter,

$$\bar{\sigma}_n = \frac{\sigma_n}{\sigma_o} = \frac{p_A + p_F}{\sigma_o} \tag{4.6}$$

which is to be added to those originally given in Eq. (4.1). Summarizing then for a material whose plastic stress-strain curve is matched by the Ramberg-Osgood approximation as stated previously, the general parameters for stress and

deflection similarity are,

$$\frac{\sigma_0}{E_0} \quad , \quad \frac{\sigma_0}{(\sigma_{.7})_0} \quad , \quad \bar{\bar{\sigma}}_{.7} \quad , \quad \alpha_0 T_0 \quad , \quad \overline{\overline{T_B}} \quad , \quad \frac{u_0}{L}$$

$$\frac{\rho_B L^2}{\sigma_0 t_0^2} \quad , \quad \frac{\rho_B g L}{\sigma_0} \quad , \quad \frac{p_A + p_F}{\sigma_0} \quad , \quad \bar{\bar{E}} \quad , \quad \bar{\bar{\alpha}} \quad , \quad \nu \tag{4.7}$$

The form of the boundary condition Eq. (4.6) as given above, permits the addition of non-aerodynamic loads p_F on a model to adjust for a purely aerodynamic loading on the prototype, provided this aerodynamic loading is known (see discussion in Section 5.1e, also see Ref. 1). If the aerodynamic loading is not known in advance, as in aeroelastic type models, it is then required to simulate both p_A/σ_0 and p_F/σ_0 separately.

For example, for such aerodynamic type testing over the surface of bodies in hypersonic flow, $p_F = 0$ and p_A/σ_0 becomes (see Eq. 2.3),

$$\frac{p_A}{\sigma_0} = \frac{\rho_\infty U^2}{\sigma_0} \bar{p} \tag{4.8}$$

Maintaining the required aerodynamic similarity $\bar{p}$ for this general body as discussed in Section 2.2, the above reduces to the condition of

$$\frac{\rho_\infty U^2}{\sigma_0} \tag{4.9}$$

which replaces the $(p_A + p_B)/\sigma_0$ condition of Eq. (4.7) for these purely aerodynamic type loadings. The similarity parameters for the combined aerodynamic, heat transfer, and stress and deflection similarity will be discussed further in Section 5.

b) Stresses and Deflections of Plates

A specific type of structure that is often encountered in aeroelastic work is the plate. Low aspect ratio wings are characteristically thin and deform much like a plate. A convenient means of representing the deflections of a wing of this type is to transform the actual structure into an equivalent plate of varying bending and extensional stiffness. It might be of interest therefore to examine the specific similarity parameters associated with heated and laterally loaded plates. See also Section 4.3 of Ref. 1 where this subject was also discussed along somewhat similar lines as given below.

The governing differential equations of a heated isotropic plate are,

$$\frac{\partial^2}{\partial x^2}\left[D\left(\frac{\partial^2 w}{\partial x^2} + \nu \frac{\partial^2 w}{\partial y^2}\right)\right] + \frac{\partial^2}{\partial y^2}\left[D\left(\frac{\partial^2 w}{\partial y^2} + \nu \frac{\partial^2 w}{\partial x^2}\right)\right] + 2\frac{\partial^2}{\partial x \partial y}\left[D(1-\nu)\frac{\partial^2 w}{\partial x \partial y}\right] \tag{4.10}$$

$$= \Delta p + \frac{\partial^2 F}{\partial y^2}\frac{\partial^2 w}{\partial x^2} + \frac{\partial^2 F}{\partial x^2}\frac{\partial^2 w}{\partial y^2} + 2\frac{\partial^2 F}{\partial x \partial y}\frac{\partial^2 w}{\partial x \partial y} - \frac{\partial^2 M_T}{\partial x^2} - \frac{\partial^2 M_T}{\partial y^2}$$

$$\frac{\partial^2}{\partial x^2}\left[\frac{1}{C(1-\nu^2)}\left(\frac{\partial^2 F}{\partial x^2}-\nu\frac{\partial^2 F}{\partial y^2}\right)\right]+\frac{\partial^2}{\partial y^2}\left[\frac{1}{C(1-\nu^2)}\left(\frac{\partial^2 F}{\partial y^2}-\nu\frac{\partial^2 F}{\partial x^2}\right)\right]+2\frac{\partial^2}{\partial x\partial y}\left[\frac{1}{C(1-\nu)}\frac{\partial^2 F}{\partial x\partial y}\right]$$

$$=\left(\frac{\partial^2 w}{\partial x\partial y}\right)^2-\frac{\partial^2 w}{\partial x^2}\frac{\partial^2 w}{\partial y^2}-\frac{\partial^2}{\partial x^2}\left[\frac{N_T}{C(1+\nu)}\right]-\frac{\partial^2}{\partial y^2}\left[\frac{N_T}{C(1+\nu)}\right] \qquad (4.11)$$

where $\Delta p(x,y,t)$ is the distributed lateral loading per unit area of the plate.

These two equations are the Von Kármán equations for large deflections of a plate with variable stiffness properties under applied loads and thermal stresses. The quantity w(x,y,t) is the lateral deflection of the neutral surface from its initial position, F is the stress function, C and D are the extensional and bending stiffness per unit length respectively, and N_T and M_T are the thermal force and moment per unit length respectively. These latter are defined more generally as,

$$C=\int_{-\delta/2}^{\delta/2}\frac{E}{1-\nu^2}\,dz\,,\qquad D=\int_{-\delta/2}^{\delta/2}\frac{Ez^2}{1-\nu^2}\,dz$$

$$N_T=\int_{-\delta/2}^{\delta/2}\frac{E\alpha\Delta T}{1-\nu}\,dz\,,\qquad M_T=\int_{-\delta/2}^{\delta/2}\frac{E\alpha\Delta T z}{1-\nu}\,dz \qquad (4.12)$$

where δ is the plate thickness and ΔT is the temperature rise from some initial value.

Introducing the following non-dimensional parameters,

$$\bar{x} = \frac{x}{L} \quad , \quad \bar{y} = \frac{y}{L} \quad , \quad \bar{w} = \frac{w}{u_o} \quad , \quad \bar{F} = \frac{F_o}{C_o L^2}$$

$$\bar{\bar{C}} = \frac{C}{C_o} \quad , \quad \bar{\bar{D}} = \frac{D}{D_o} \quad , \quad \bar{\bar{N}}_T = \frac{N_T}{N_{T_o}} \quad , \quad \bar{\bar{M}}_T = \frac{M_T}{M_{T_o}} \tag{4.13}$$

the Von Kármán equations become,

$$\frac{\partial^2}{\partial \bar{x}^2}\left[\bar{\bar{D}}\left(\frac{\partial^2 \bar{w}}{\partial \bar{x}^2} + \nu \frac{\partial^2 \bar{w}}{\partial \bar{y}^2}\right)\right] + \cdots = \frac{L^4 \Delta p}{D_o u_o} \tag{4.14}$$

$$+ \left(\frac{C_o L^2}{D_o}\right)\left[\frac{\partial^2 \bar{F}}{\partial \bar{y}^2} \frac{\partial^2 \bar{w}}{\partial \bar{x}^2} + \cdots\right] - \left(\frac{L^2 M_{T_o}}{u_o D_o}\right)\left[\frac{\partial^2 \bar{\bar{M}}_T}{\partial \bar{x}^2} + \frac{\partial^2 \bar{\bar{M}}_T}{\partial \bar{y}^2}\right]$$

$$\frac{\partial^2}{\partial \bar{x}^2}\left[\frac{1}{\bar{\bar{C}}(1-\nu)}\left(\frac{\partial^2 \bar{F}}{\partial \bar{x}^2} - \nu \frac{\partial^2 \bar{F}}{\partial \bar{y}^2}\right)\right] + \cdots = \left(\frac{u_o^2}{L^2}\right)\left[\frac{\partial^2 \bar{w}}{\partial \bar{x} \partial \bar{y}} + \frac{\partial^2 \bar{w}}{\partial \bar{x}^2} \frac{\partial^2 \bar{w}}{\partial \bar{y}^2}\right] \tag{4.15}$$

$$- \left(\frac{N_{T_o}}{C_o}\right)\left[\frac{\partial^2}{\partial \bar{x}^2}\left(\frac{\bar{\bar{N}}_T}{\bar{\bar{C}}(1+\nu)}\right) + \frac{\partial^2}{\partial \bar{y}^2}\left(\frac{\bar{\bar{N}}_T}{\bar{\bar{C}}(1+\nu)}\right)\right]$$

The first non-dimensional parameter appearing above, $L^4 \Delta p / D_o u_o$ may be split up further by noting that the lateral loading Δp may be due to aerodynamic, inertial, gravity, or externally applied forces

$$\Delta p = p_A - m\frac{\partial^2 w}{\partial t^2} - mg + p_F \tag{4.16}$$

Hence the resulting non-dimensional parameters for a plate under lateral loads and varying temperature are

$$\frac{L^4 p_A}{D_o u_o}\ ,\ \frac{m_o L^4}{D_o t_o^2}\ ,\ \frac{m_o g L^4}{D_o u_o}\ ,\ \frac{p_F L^4}{D_o u_o}\ ,\ \frac{C_o L^2}{D_o}$$
$$\frac{L^2 M_{T_o}}{D_o u_o}\ ,\ \frac{u_o}{L}\ ,\ \frac{N_{T_o}}{C_o}\ ,\ \nu\ ,\ \bar{\bar{C}}\ ,\ \bar{\bar{D}}\ ,\ \bar{\bar{N}}_T, \bar{\bar{M}}_T, \bar{\bar{m}} \tag{4.17}$$

For the study of small deflections, w, of heated plates, the nonlinear terms $(\partial^2 w/\partial x \partial y)^2 - (\partial^2 w/\partial x^2)(\partial^2 w/\partial y^2)$ appearing in Eq. (4.11) may be neglected. In this case the u_o/L requirement in Eq. (4.15) would not appear. Further, it is seen that this would then uncouple the two equations and permit one to solve the second equation for the stress function in the form,

$$\bar{F} = \frac{N_{T_o}}{C_o}\ \bar{q}(\bar{x}, \bar{y}) \tag{4.18}$$

where $\bar{q}(\bar{x}, \bar{y})$ is some non-dimensional function depending on the temperature distribution and boundary conditions of the plate. Placing this back into the first equation for $\bar{w}$ would result in the following non-dimensional parameters for the small deflections of a heated, laterally loaded plate

$$\frac{L^4 p_A}{D_o u_o}\ ,\ \frac{m_o L^4}{D_o t_o^2}\ ,\ \frac{m_o g L^4}{D_o u_o}\ ,\ \frac{p_F L^4}{D_o u_o}\ ,\ \frac{N_{T_o} L^2}{D_o}$$
$$\frac{L^2 M_{T_o}}{D_o u_o}\ ,\ \nu\ ,\ \bar{\bar{C}}\ ,\ \bar{\bar{D}}\ ,\ \bar{\bar{N}}_T\ ,\ \bar{\bar{M}}_T\ ,\ \bar{\bar{m}} \tag{4.19}$$

4.2 Long-Time Loading

In this category the duration of loading is sufficiently long that time under load will appear as an additional parameter relating to such items as creep and fatigue. The consideration of time under load as a parameter is in addition to requiring the reproduction of the parameters of Eq. (4.1) and Eq. (4.6) for similitude. Reproduction of the actual time experienced by a prototype for a given loading will in most cases be impossible because of the short operating times of wind tunnels. Furthermore, if the actual time spent at temperature is important for a transient temperature test, this too is impractical to reproduce since simulation of the transient heating problem (for same materials for example, Eq. 3.6) requires the time scale to be reduced according to

$$\frac{(t_o)_M}{(t_o)_P} = \left(\frac{L_M}{L_P}\right)^2 \tag{4.20}$$

For a steady-state heating experiment this last restriction however does not apply.

Reproduction of strain-rate is important since it affects the creep and fatigue behavior of a structure. Therefore it is important to consider both the load level and the rate of loading of a heated structure along with the thermal loading.

Duplication of the aforementioned long-time loading effects on a one-to-one time basis is impossible in practically all cases if wind tunnel testing is utilized. Certain alternatives are available however. It is possible,

at least for structures in which a two dimensional state of stress exists, to utilize results of phenomena such as creep, tension and compression loadings at short periods of time and given stress and temperature levels to extrapolate to longer periods of time and different stress and temperature levels with the Larson-Miller parameter

$$T(C + \log t) \tag{4.21}$$

where C is a constant characteristic of the material and t is the time to rupture or to achieve a given strain (Ref. 27). This parameter has correlated data over a wide range of times and temperatures for many steels, high temperature alloys, and aluminium alloys.

Another alternative is to utilize short-time experimental data in a cummulative sense. As suggested by Gerard (Ref. 28) for creep, the total cummulative creep may be taken as the sum of the creep increments due to the time spent at each stress and temperature level. The creep deformation of a prototype, to a first approximation, may thus be accounted for by conducting several model tests at a given load and temperature level where the total testing time is equal to the prototype time.

The problem of fatigue at present is not well understood, especially at elevated temperatures. However, some current experimental techniques can be suggested here. The cumulative-damage theory of Miner (Ref. 29) may be used to correlate fatigue data for several tests each run for a different number of cycles n_i at a specified stress and temperature level with which a fatigue life N is associated. According to this theory, the fatigue life of a prototype will be reproduced experimentally if

$$\left(\frac{n_1}{N_1} + \frac{n_2}{N_2} + \cdots\right)_M = \left(\frac{n_1}{N_1} + \frac{n_2}{N_2} + \cdots\right)_P \qquad (4.22)$$

where each term on the left side above represents a model test and each term on the right represents the percentage of time spent by the prototype at any given stress level. The fatigue life N at each stress level would have to be obtained from an $\sigma - N$ diagram at the corresponding temperature level. The cumulative damage concept is based on the assumption that the cycling tests may be conducted in any desireable sequence with no effect on the fatigue life.

An alternative method consists of determining an equivalent stress σ_r of constant amplitude which would have the same overall effect as a variable loading at different stress levels $\sigma_1, \sigma_2, \cdots$, and at different cycles $n_1, n_2, \cdots$, (Ref. 29). This equivalent stress σ_r may be expressed as

$$\sigma_r = \frac{\sigma_1^x n_1 + \sigma_2^x n_2 + \cdots}{n_1 + n_2 + \cdots} \qquad (4.23)$$

where the exponent x is the inverse slope of the $\sigma - N$ diagram on a log-log plot. The equivalent stress σ_r of the prototype may be estimated and then a series of tests may be conducted on the model at various stress levels and cycles satisfying Eq. (4.23) and the condition $(\sigma_r)_m = (\sigma_r)_p$.

Additional considerations are important when dealing with fatigue. Scale effect may be very significant but the extent of this has not been fully understood. One theory holds that a specimen in which a large volume is

subjected to high stress has more chance of containing a weak spot that determines failure than does a smaller piece (Ref. 30). Reproduction of geometric details and use of the same material is also necessary.

For the problems discussed in this category it appears desirable that wherever possible the applied load and temperature spectrums of a model should be the same as the prototype. In many cases this will not be possible and some of the suggestions mentioned above may be applied, accounting for these phenomena at least in an approximate manner.

5. SIMILARITY REQUIREMENTS FOR COMBINED AERODYNAMIC, HEAT CONDUCTION, AND STRESS-DEFLECTION STUDIES

In the previous sections the similarity laws required for studying in detail the aerodynamic pressure distribution, aerodynamic heat transfer, structural heat transfer, and stress-deflection phenomena at hypersonic Mach numbers have been discussed individually. It was indicated there what similarity parameters can be expected in a particular "restricted purpose" test. Thus, for example, the parameters of Eq. (2.10) are sufficient for studying the inviscid flow field about rigid sharp-nosed slender bodies, the parameters of Eq. (2.14) for viscous interaction effects, either Eq. (2.31) or (2.33) for studying the heat transfer rate at the stagnation point, Eq. (3.40) for ascertaining the heat blocking effectiveness of ablative materials and Eq. (4.1) for short-time stress-deflection behavior.

In the present section, the combined similarity of these phenomena as desired for complete aerothermoelastic testing will be discussed. Detailed combined simulation will not be possible in most cases. It is hoped however, to bring out the more significant parameters for these tests, and to illustrate their application to boost glide and ballistic type vehicles.

5.1 General Features

The similarity parameters required generally for a complete aerothermoelastic model placed in a perfect gas hypersonic flow may be summarized from Eqs. (2.5), (2.28), (3.32), (4.1) and (4.6) as

$$Re_s \;,\; P_{rs} \;,\; \gamma \;,\; \frac{T_0}{U^2/2C_{p_s}} \;,\; \frac{Ut_0}{L} \;,\; \bar{\bar{\mu}} \;,\; \bar{\bar{C}}_p \;,\; \bar{\bar{k}}$$

$$\frac{A_s}{K_0} \;,\; \frac{\epsilon_0 T_0^3 L}{K_0} \;,\; \frac{\pi_0 t_0}{L^2} \;,\; \bar{\bar{K}}_B \;,\; \bar{\bar{C}}_{p_B} \;,\; \bar{\bar{\rho}}_B \;,\; \frac{T_M}{T_0}$$

$$\frac{LM}{C_{p_0} T_0} \;,\; \frac{(P_{rs})^{2/3} K_0 T_0 L}{U \mu_0 \pi_0} \;,\; \frac{\rho_\infty U^2 L^2}{\mu_0 \pi_0} \;,\; \frac{V_0 L}{\pi_0} \;,\; \frac{T_v}{T_0} \qquad (5.1)$$

$$\frac{L_v + \eta(h_s - h_v)}{C_{p_0} T_0} \;,\; \bar{\bar{K}}_L \;,\; \bar{\bar{C}}_{p_L} \;,\; \bar{\bar{\rho}}_L \;,\; \bar{\bar{\mu}}_L \;,\; \frac{\rho_\infty U^2}{E_0}$$

Shape of stress-strain curve, $\alpha_0 T_0$, $\frac{u_0}{L}$, $\frac{\rho_B L^2}{\rho_\infty U^2 t_0^2}$

$$\frac{\rho_B g L}{\rho_\infty U^2} \;,\; \frac{\rho_\infty U^2}{\sigma_0} \;,\; \frac{P_F}{\sigma_0} \;,\; \bar{\bar{E}} \;,\; \bar{\bar{\alpha}} \;,\; \nu$$

The model should possess complete geometric similarity. The significance of each of the above parameters has already been discussed in Sections 2,3 and 4. If the above similarity conditions are all met, the following non-dimensional quantities will be the same on both model and prototype,

$$\frac{P}{\rho_\infty U^2} \;,\; \frac{T}{T_0} \;,\; \frac{\sigma}{\sigma_0} \;,\; \frac{t}{t_0} \;,\; \frac{u_{(VELOCITY)}}{U} \;,\; \frac{u_{(DISPLACEMENT)}}{u_0} \qquad (5.2)$$

and measurements on the model can infer behavior of the full scale prototype. The arbitrary reference values T_0, σ_0, t_0 and u_0 may differ on both model and prototype,

but must be consistent with the 4th, 5th, 11th, 29th, 30th, and the 32nd similarity conditions of Eq. (5.1), respectively.

The parameters of Eq. (5.1) are to be compared with those of the lower supersonic range given in Section 2.4 of Ref. 1. The absence of the Mach number condition in Eq. (5.1) is to be noted for these hypersonic speeds.

The parameters of Eq. (5.1) apply aerodynamically to a perfect gas. As mentioned in Section 2.1, because of the high temperatures involved, real gas effects come into play and in order to simulate these, the same temperatures and same pressures in the same gas should be maintained on model and prototype. This then requires adding the parameters

$$U, \quad \rho_\infty, \text{ same gas} \tag{5.3}$$

to the list of Eq. (5.1). Further, to account for the variation in material properties over these wide temperature ranges (such items as $\bar{\bar{K}}_\theta$, $\bar{\bar{C}}_{\rho_\theta}$, $\bar{\bar{E}}$ shape of stress-strain curve, etc.) it would be desirable also to use the same material for both model and prototype. For similar temperatures, pressures and materials then, the parameters of Eqs. (5.3) and (5.1) reduce to

$$\begin{gathered} U, \ \rho_\infty, \text{ same gas}, \ Re_s = L, \ \frac{t_o}{L}, \ \epsilon_o L \\ \frac{t_o}{L^2}, \ L, \ L^2, \ V_o L, \ \frac{u_o}{L}, \ gL, \ \sigma_o, \ \rho_F \end{gathered} \tag{5.4}$$

A fundamental conflict appears here in the Reynolds number Re_s, condition. This cannot be satisfied now for anything

other than unity scale ratio*. It appears then that general similarity cannot be achieved, and that recourse must be made to less restrictive specialized situations.

a) Blunt-Nosed Body

Consider first the aerothermoelastic similarity in the neighborhood of the nose of a blunt body. From Eqs. (2.6), (2.31), (3.32), (4.1) and (4.6), the similarity requirements are effectively

$$\begin{gathered}
\frac{k_s}{K_0}\sqrt{R_{e_s}}\,P_{r_s}^{.4}\,\frac{h_s}{c_{p_s}T_0}\left\{\left(\frac{\gamma+3}{\gamma+1}\right)^{.5}\left(\frac{\gamma}{\gamma-1}\right)^{.25}\left(\frac{\rho_w\mu_w}{\rho_s\mu_s}\right)^{.1}\right\}\left[1+(Le^{\eta}-1)\frac{h_D}{h_s}\right],\ \frac{Ut_0}{L}\\
\frac{\epsilon_0 T_0^3 L}{K_0},\ \frac{\pi_0 t_0}{L^2},\ \bar{\bar{K}}_B,\ \bar{\bar{C}}_{p_B},\ \bar{\bar{\rho}}_B,\ \frac{T_M}{T_0},\ \frac{L_M}{C_{p_0}T_0},\ \frac{(P_{r_s})^{2/3}K_0T_0L}{U\mu_0\pi_0}\\
\frac{\rho_\infty U^2L^2}{\mu_0\pi_0},\ \frac{V_0L}{\pi_0},\ \frac{T_v}{T_0},\ \frac{L_v+\eta(h_s-h_v)}{C_{p_0}T_0},\ \bar{\bar{K}}_L,\ \bar{\bar{C}}_{p_L},\ \bar{\bar{\rho}}_L\\
\bar{\bar{\mu}}_L,\ \frac{\rho_\infty U^2}{E_0},\ \text{shape of stress-strain curve},\ \alpha_0T_0,\ \frac{u_0}{L},\\
\frac{\rho_0L^2}{\rho_\infty U^2t_0^2},\ \frac{\rho_B\,qL}{\rho_\infty U^2},\ \frac{\rho_\infty U^2}{\sigma_0},\ \frac{\rho_F}{\sigma_0},\ \bar{\bar{E}},\ \bar{\bar{\alpha}},\ \nu
\end{gathered}\tag{5.5}$$

Here, the first combined parameter above replaces eight of the first nine parameters of Eq. (5.1). The { } and [ ] quantities do not vary much, and it is assumed that $T_w \ll T_s$.

*The other L conditions in the 8th and 9th parameters are not as important, as they stem from the detailed ablation flow requirements. Also the t_0/L and t_0/L^2 conditions can be somewhat circumvented by dealing with two different time scales, one for unsteady aerodynamic phenomena and another for heat conduction phenomena. These are usually fairly well separated and do not cause much coupling.

There is now no aerodynamic requirement of maintaining same temperatures and same pressures in the gas. However, to account for variation in material properties and for ablation, it would be desirable to utilize the same materials at the same temperatures. Under these conditions, the requirements of Eq. (5.5) reduce to

$$\frac{\sqrt{\rho_\infty U L \mu_s}}{(Pr_s)^{.6}} h_s \left\{\left(\frac{\gamma+3}{\gamma+1}\right)^{.5}\left(\frac{\gamma}{\gamma-1}\right)^{.25}\left(\frac{\rho_w \mu_w}{\rho_s \mu_s}\right)^{.1}\right\}\left[1+(Le^{n}-1)\frac{h_D}{h_s}\right], \frac{U t_0}{L}$$

$$\epsilon_0 L, \quad \frac{t_0}{L^2}, \quad \frac{(Pr_s)^{2/3} L}{U}, \quad \rho_\infty U^2 L^2, \quad V_0 L, \quad \eta h_s, \tag{5.6}$$

$$\rho_\infty U^2, \quad \frac{u_0}{L}, \quad \frac{t_0}{L}, \quad gL, \quad r_0, \quad p_F$$

The first parameter (basic aerodynamic requirement) can now be made compatible with the ninth parameter ($\rho_\infty U^2$ requirement), thereby permitting similarity for a non-ablating body. Note that if the stagnation enthalpy is due to velocity alone, $h_s \approx U^2/2$ *. Two of the ablation parameters (the fifth and sixth above) cannot be met however, thereby excluding detailed ablation similarity for this case. As can be seen from Section 3.2, however, these two ablation parameters relate to the flow of the melted layer. If the ablation process is such that the melted layer is removed very quickly, these parameters will not play much of a role and hence may be neglected. Also, the unsteady aerodynamic parameter Ut_0/L might be difficult to reconcile with the t_0/L condition associated with the structural vibrations in a dynamic aeroelastic test.

*In shock tube, the stagnation enthalpy $h_s > U^2/2$.

b) Non-ablating Slender Bodies (same γ)

For the aerothermoelastic similarity of slender bodies of the same thickness ratio γ , the similarity parameters as obtained from Eqs. (2.14), (2.18), (2.37), (3.12), (4.1) (4.6) and (4.9) are

$$M_\infty \;,\; \gamma \;,\; \frac{u_0}{L} \;,\; \frac{U t_0}{L} \;,\; \sqrt{\frac{\rho_\infty U L}{\mu_s}}$$

$$\frac{T_w}{T_s} \;,\; P_r \;,\; M_\infty^3 k \frac{d}{L} \;,\; \frac{k_s}{K_0}\sqrt{\frac{\rho_\infty U L}{\mu_s}}\, P_{rs}\, \frac{h_s}{c_{p_s} T_0}$$

$$\frac{\epsilon_0 T_0^3 L}{K_0} \;,\; \frac{\pi_0 t_0}{L^2} \;,\; \bar{\bar{K}}_B \;,\; \bar{\bar{c}}_{p_B} \;,\; \bar{\bar{\rho}}_B \;,\; \frac{\rho_\infty U^2}{E_0} \qquad (5.7)$$

shape of stress-strain curve , $\alpha_0 T_0$,

$$\frac{\rho_B L^2}{\rho_\infty U^2 t_0^2} \;,\; \frac{\rho_B g L}{\rho_\infty U^2} \;,\; \frac{\rho_\infty U^2}{\sigma_0} \;,\; \frac{\rho_F}{\sigma_0} \;,\; \bar{\bar{E}} \;,\; \bar{\bar{\alpha}} \;,\; \nu$$

The first parameter can be dropped if $M_\infty \gamma \gg 1$ for both model and prototype. There is now only a weak aerodynamic requirement to maintain same temperatures and pressures in the gas stemming from viscous boundary layer interaction effects (the fifth, sixth, and seventh parameters above). However, to account for variation in material properties, it would be desirable to keep the temperatures the same on model and prototype. Under these conditions, the

parameters of Eq. (5.7) reduce to

$$\gamma\,,\ \frac{u_0}{L}\,,\ \frac{Ut_0}{L}\,,\ \sqrt{\frac{\rho_\infty UL}{\mu_S}}\,,\ T_S\,,\ P_r\,,$$

$$M_\infty^3 k\frac{d}{L}\,,\ \sqrt{\rho_\infty UL\mu_S}\,h_S\,,\ \epsilon_0 L\,,\ \frac{t_0}{L^2} \qquad (5.8)$$

$$\rho_\infty U^2\,,\ \frac{t_0}{L}\,,\ gL\,,\ \sigma_0\,,\ P_F$$

The above are somewhat similar to the requirements for the blunt body, Eq. (5.6). The T_S condition above, if adhered to would generally require similar velocities U. For $T_w \ll T_S$ and for small viscous interaction effects, this T_S condition along with the $\sqrt{\rho_\infty UL/\mu_S}$ and P_r conditions can be disregarded, thereby allowing more freedom to satisfy the parameters of Eq. (5.8) much in the same way as those of the blunt body, Eq. (5.6).

The parameters of Eq. (5.7), although obtained specifically for slender bodies, apply also for arbitrary bodies if the Prandtl boundary layer assumption is reasonable and there is not much viscous interaction. For such bodies, the viscous interaction parameters (fourth to sixth above) can be disregarded, and the pressure distribution is controlled essentially by M_∞, γ, u_0/L. The aerodynamic heating is essentially controlled by the $(k_S/k_0)\sqrt{Re_S}\,P_{r_S}\,(h_S/c_{p_S}T_0)$ condition. See for example, Section 2.3b. The heating here has been assumed laminar. If it is turbulent, Eq. (2.35b) would be used in place of Eq. (2.35a) above. Again, the unsteady aerodynamic parameter Ut_0/L might be difficult to reconcile with the t_0/L condition associated with the structural vibrations in a dynamic aeroelastic test.

c) Non-ablating Slender Bodies (different τ)

For a family of affinely related slender lifting surfaces of differing thickness ratios, aerothermoelastic similarity can be achieved under certain conditions. It will be assumed that,

1) Model and prototype are affinely related thin solid plates of differing thickness ratios τ.

2) A flutter or static aeroelastic type test is envisaged.

3) Small deflection plate theory is applicable.

4) Heat flow into the thin plate causes a very small temperature variation through the thickness of the plate.

Under these conditions, the similarity parameters are obtained from Eqs. (2.14), (2.18), (2.36), (3.12), (4.19) and (2.8), as

$$M_\infty \tau,\ \gamma,\ \frac{u_0}{L\tau},\ \frac{U t_0}{L},\ \tau^2\sqrt{\frac{\rho_\infty U L}{\mu_s}},\ \frac{T_w}{T_s},$$

$$P_r,\ M_\infty^3 A \frac{d}{L},\ \frac{A_s}{K_0}\sqrt{\frac{\rho_\infty U L}{\mu_s}}\,P_{r_s}\,\frac{h_s}{c_{p_s} T_0},\ \frac{\epsilon_0 T_0^3 L}{K_0 \tau} \qquad (5.9)$$

$$\frac{m_0 t_0}{L^2},\ \bar{\bar{K}}_B,\ \bar{\bar{C}}_{P_B},\ \bar{\bar{\epsilon}}_w,\ \frac{L^4 \rho_\infty U^2 \tau^2}{D_0 u_0}$$

$$\frac{m_0 L^4}{D_0 t_0^2},\ \frac{m_0 g L^4}{D_0 u_0},\ \frac{N_{T_0} L^2}{D_0},\ \frac{L^2 M_{T_0}}{D_0 u_0},\ \nu,\ \bar{\bar{m}}$$

For a thin solid plate

$$D_o = \left[\frac{E\delta^3}{12(1-\nu^2)}\right]_o = \frac{E_o \gamma^3 L^3}{12(1-\nu^2)}$$

$$C_o = \left[\frac{E\delta}{1-\nu^2}\right]_o = \frac{E_o \gamma L}{1-\nu^2} \qquad (5.10)$$

$$N_{T_o} = \left[\frac{E\alpha\Delta T\,\delta}{1-\nu}\right]_o = \frac{E_o \alpha_o \Delta T_o \gamma L}{1-\nu}$$

$$M_{T_o} = 0$$

where $\bar{\bar{\delta}}$ is simulated by the condition of affinely related bodies. Placing the above into the parameters of Eq. (5.9) and rearranging gives

$$M_\infty \gamma,\quad \gamma,\quad \frac{u_o}{L\gamma},\quad \frac{Ut_o}{L},\quad \gamma^2\sqrt{\frac{\rho_\infty UL}{\mu_s}},\quad \frac{T_w}{T_g},$$

$$P_r,\quad M_\infty^3 k\frac{d}{L},\quad \frac{k_s}{K_o}\sqrt{\frac{\rho_\infty UL}{\mu_s}}\,P_{r_s}\frac{h_s}{c_{p_s}T_o},\quad \frac{\epsilon_o T_o^3 L}{K_o\gamma}, \qquad (5.11)$$

$$\frac{K_o t_o}{L^2},\quad \bar{\bar{K}}_s,\quad \bar{\bar{C}}_{p_\theta},\quad \bar{\bar{\epsilon}}_w,\quad \frac{\rho_\infty U^2}{E_o\gamma^2},\quad \frac{\rho_\theta L^2}{\rho_\infty U^2 t_o^2}$$

$$\frac{qL}{\gamma U^2},\quad \frac{\alpha_o T_o}{\gamma^2},\quad \nu,\quad \bar{\bar{E}},\quad \bar{\bar{\alpha}}$$

The $M_\infty\gamma$ condition may be dropped if $M_\infty\gamma \gg 1$. The fifth, sixth, and seventh parameters above refer to viscous boundary layer interaction effects and may be dropped if these effects are small.

If it is desired to keep the same temperatures in both model and prototype, the thermal stress condition $\alpha_0 T_0/\gamma^2$ would require the same thickness ratio γ for model and prototype made of the same material. The parameters of Eq. (5.11) are then seen to reduce to those of the general body given previously by Eq. (5.7).

d) Free Molecule Flow

For a blunt body in high speed free molecule flow, the aerothermoelastic similarity parameters are obtained from Eqs. (2.23), (2.45), (2.49), (3.6), (4.1), and (4.6), namely,

$$\frac{a_e \rho_\infty U^3 L}{K_0 T_0}\ ,\ \frac{g_{SOL} L}{K_0 T_0},\ \frac{g_{AERL} L}{K_0 T_0}\ ,\ \frac{\epsilon_0 T_0^3 L}{K_0}\ ,\ \frac{\pi_0 t_0}{L^2}\ ,\ \frac{U t_0}{L}$$

$$\bar{\bar{K}}_B\ ,\ \bar{\bar{C}}_{P_B}\ ,\ \bar{\bar{\epsilon}}_w\ ,\ \frac{\rho_\infty U^2}{E_0} \qquad \text{shape of stress-strain curve,} \tag{5.12}$$

$$\alpha_0 T_0\ ,\ \frac{u_0}{L}\ ,\ \frac{\rho_B L^2}{\rho_\infty U^2 t_0^2}\ ,\ \frac{\rho_B g L}{\rho_\infty U^2}\ ,\ \frac{\rho_\infty U^2}{\sigma_0}$$

$$\frac{P_F}{\sigma_0}\ ,\ \bar{\bar{E}}\ ,\ \bar{\bar{\alpha}}\ ,\ \nu$$

In the above case, it is not likely that very high temperatures or plastic stresses will be reached. Hence, working with the same material at the same temperatures is not necessary here, and some flexibility may be achieved by using different materials and different reference temperatures T_0 .

For slender bodies, of the same thickness ratio γ , the corresponding parameters as obtained from Eqs. (2.24), (2.47), (2.49), (3.6), (4.1) and (4.6) are the same as Eq. (5.12) above plus the additional parameters

$$S\ ,\ \frac{T_w}{T_s}\ ,\ f \tag{5.13}$$

For very high speeds such that $S\gamma \gg 1$, the above parameters drop out leaving only those of Eq. (5.12) again.

For affinely related slender bodies of differing thickness ratio γ, aerothermoelastic similarity can be achieved subject to the assumptions mentioned in Section 5.1c. Under these conditions, the similarity parameters as obtained from Eqs. (2.24), (2.47), (2.49), (3.12), (4.19), and (2.21) are

$$S\gamma\,,\quad \frac{T_w}{T_\infty}\,,\quad f\,,\quad \frac{u_0}{L\gamma}\,,\quad \frac{Ut_0}{L}\,,\quad \frac{q_e \rho_\infty U^3 L}{K_0 T_0}\,,\quad \frac{q_{SOL} L}{K_0 T_0 \gamma}$$

$$\frac{q_{EAR} L}{K_0 T_0 \gamma}\,,\quad \frac{\epsilon_0 T_0^3 L}{K_0 \gamma}\,,\quad \frac{\pi_0 t_0}{L^2}\,,\quad \bar{\bar{K}}_\theta\,,\quad \bar{\bar{C}}_{f_\theta}\,,\quad \bar{\bar{\epsilon}}_w\,,\quad \frac{\rho_\infty U^2}{E_0 \gamma^2} \qquad (5.14)$$

$$\frac{\rho_\theta L^2}{\rho_\infty U^2 t_0^2}\,,\quad \frac{gL}{\gamma U^2}\,,\quad \frac{\alpha_0 T_0}{\gamma^2}\,,\quad \bar{\bar{E}}\,,\quad \bar{\bar{\alpha}}\,,\quad \nu$$

Again for $S\gamma \gg 1$, the first three parameters would drop out. Also, for the same temperatures in both model and prototype material, the $\alpha_0 T_0/\gamma^2$ condition requires the same γ, and the above reduces to the conditions of Eq. (5.12). It is to be noted, in free molecule flow, the temperatures are not apt to become very high. It is then not so necessary to reproduce the same materials and the same temperatures as it would be if higher operating temperatures are present.

e) Incomplete Aerothermoelastic Testing

By incomplete aerothermoelastic testing is meant here the use of other auxiliary means than just the air stream alone to provide the net aerodynamic pressure input p_{NET} and the net heat transfer input q_{NET} to the model structure. This requires a priori knowledge of what these loadings p_{NET} and q_{NET} will be on the prototype. In all

the preceding similarity investigations of Section 5, a complete aerothermoelastic model was envisaged, i.e., one which when immersed in a high speed flow would simulate automatically the proper aerodynamic pressure and aerodynamic heating environment of the prototype. Since as was seen it is difficult to obtain complete aerothermoelastic models except in certain specialized situations, recourse can be had as a last resort to the cruder incomplete aerothermoelastic testing.

Looking at the problem of a body subjected to a general force distribution p_{NET} and a general heating rate q_{NET}, the similarity parameters may be summarized from Eqs. (3.10), (3.30), (4.1), and (4.6) as

$$\frac{q_{NET}L}{K_0 T_0}, \quad \frac{\pi_0 t_0}{L^2}, \quad \bar{\bar{K}}_B, \quad \bar{\bar{C}}_{p_B}, \quad \frac{T_M}{T_0}, \quad \frac{L_M}{C_{p_0} T_0},$$

$$\frac{\gamma_A L}{\mu_0 V_0}, \quad \frac{p_{NET}L}{\mu_0 V_0}, \quad \frac{V_0 L}{\pi_0}, \quad \frac{T_V}{T_0}, \quad \frac{L_V}{C_{p_0} T_0}, \quad \bar{\bar{K}}_L \tag{5.15}$$

$$\bar{\bar{C}}_{p_L}, \quad \bar{\bar{\rho}}_L, \quad \bar{\bar{\mu}}_L, \quad \frac{p_{NET}}{E_0}, \text{ shape of stress-strain curve,}$$

$$\alpha_0 T_0, \quad \frac{u_0}{L}, \quad \frac{\rho_B L^2}{\sigma_0 t_0^2}, \quad \frac{\rho_B g L}{\sigma_0}, \bar{\bar{E}}, \bar{\bar{\alpha}}, \nu, \quad \frac{p_{NET}}{\sigma_0}$$

In the above, the first four parameters stem from the heat conduction requirements, the fifth to fifteenth from the ablation requirements, and the remaining from the stress and deflection requirements. The net inputs to the system are defined as

$$\begin{aligned} p_{NET} &= p_A + p_F \\ q_{NET} &= q_A - \epsilon_w \sigma T_w^4 - \dot{m}_v \eta (h_s - h_w) + q_F \end{aligned} \tag{5.16}$$

where p_F and q_F are any additional pressures and heating rates to be applied to the model in order to satisfy the basic input parameters above,

$$\frac{p_{NET}}{E_o} \quad , \quad \frac{q_{NET} L}{K_o T_o} \tag{5.17}$$

on both model and prototype. In evaluating p_{NET} and q_{NET}, estimates must be made of the expected values of aerodynamic pressure p_A , aerodynamic heating rate q_A , radiation loss $\epsilon_w \sigma T_w^4$, and heat blockage due to vapor injection $\dot{m}_v \eta (h_s - h_w)$ for both prototype and model. It is for this reason that the above testing procedure is called incomplete aerothermoelastic testing. Despite these limitations, this procedure is much used for structural testing at high temperatures.

For the same materials at the same temperatures, the above parameters reduce to

$$q_{NET} L \quad , \quad \frac{t_o}{L^2} \quad , \quad \frac{\gamma_A L}{V_o} \quad , \quad \frac{L}{V_o} \quad , \quad V_o L$$

$$p_{NET} \quad , \quad \frac{u_o}{L} \quad , \quad \frac{t_o}{L} \quad , \quad qL \quad , \quad \sigma_o \tag{5.18}$$

If there is no ablation, or if the melt layer is removed very rapidly, the third, fourth, and fifth parameters above which relate to flow of the melted layer may be neglected.

In aeroelastic type model tests, it is generally difficult to add additional forces p_F to the model. In these cases, it is expedient to simulate the p_{NET} completely by aerodynamic forces p_A . As seen in Section 2.2 this means generally that $p_{NET} = p_A = \rho_\infty U^2 \bar{p}$ where the non-dimensional pressure $\bar{p}$ would be simulated by maintaining the

parameters of say Eqs. (2.6), (2.10), (2.11), (2.14) (2.15), (2.23), (2.24), and (2.25), which ever is felt to be more appropriate (usually for gross pressure effects, the viscous interaction and surface temperature effects can be neglected). The conditions of Eq. (5.15) (say for the same material at the same temperatures) would become then

$$\begin{matrix} q_{NET}L\,, & \frac{t_0}{L^2}\,, & \frac{\gamma_A L}{V_0}\,, & \frac{L}{V_0}\,, & V_0 L \\ \rho_\infty U^2\,, & \frac{u_0}{L}\,, & \frac{t_0}{L}\,, & gL\,, & \sigma_0\,, \bar{p} \end{matrix} \qquad (5.19)$$

Thus, in such an aerodynamic test, the dynamic pressure $\rho_\infty U^2$ is essentially matched.* The matching of the heat input $q_{NET}L$ might be achieved by additional q_F added to the model, say by radiant heaters in the tunnel walls.** The accurate distribution of the heating rate over the model might present some difficulty. It is to be noted however, that adding heat q_F would probably be easier than adding forces p_F particularly in a dynamic aeroelastic test where p_F would have to vary largely and rapidly with time, whereas q_F remains fairly constant with time.

5.2 Application to Boost Glide Vehicles

The similarity requirements for two specific flight trajectories will now be considered, namely the boost glide vehicle and the ballistic missile. The areas of interest for these vehicles are shown as regions II and III on the corridor plot of Fig. 1. Typical aerodynamic conditions for each vehicle are given in Fig. 2 (taken from Ref. 4), thereby illustrating the orders of magnitude of the stagnation temper-

*Other items such as M_∞ may enter implicitly through $\bar{p}$ if the Mach number is not very high.

**Tests of this nature have been reported in Ref. 37, for example.

ature, Reynolds number per foot, Mach number and velocity that may be expected for each prototype. The significant differencesbetween the two trajectories are the higher altitude, and hence lower Reynolds number, lower attendant heating rates, and longer duration of heating for the boost glide vehicle compared with the ballistic missile.

The boost glide vehicle, because of its lower aerodynamic heating rates and longer duration of flight time, would probably use radiation as a principal means of heat protection. It is also apt to be a vehicle with slender lifting surfaces. The parameters of Eqs. (5.7) and (5.8) would then be appropriate. (It is assumed that both model and prototype operate at $M_\infty \tau \gg 1$.) Considering first the case of the same materials at the same temperatures, Eq. (5.8) yields the following primary significant parameters for matching,

$$\frac{u_0}{L}\ ,\ \frac{Ut_0}{L}\ ,\ \sqrt{\rho_\infty U L \mu_s}\, h_s\ ,\ \epsilon_0 L\ ,\ \frac{t_0}{L^2}$$

$$\rho_\infty U^2\ ,\ \frac{t_0}{L}\ ,\ \nu\ ,\ \sigma_0 \qquad (5.20)$$

the others being somewhat secondary (viscous interaction effects, gravity effects, $T_s \gg T_w$, etc.). The above parameters could be matched except for the radiation condition $\epsilon_0 L$, and unsteady aerodynamic parameter Ut_0/L, by picking

$$\frac{U_M}{U_P} = \left[\frac{(\mu_s)_P L_P}{(\mu_s)_M L_M}\right]^{1/3}$$

$$\frac{(\rho_\infty)_M}{(\rho_\infty)_P} = \left(\frac{U_P}{U_M}\right)^2 \qquad (5.21)$$

In the above, the stagnation enthalpy h_s was assumed caused by velocity alone, i.e., $h_s \approx U^2/2$. The two characteristic times t_o from the fifth and seventh conditions above are associated with two different phenomena, heating and aeroelasticity respectively, and would not generally cause any coupling (see footnote Section 5.1). However, the satisfaction of the Ut_o/L condition from unsteady aerodynamics together with the t_o/L condition from the structural dynamics would not be possible unless U were the same. For static aeroelastic phenomena of course, both these could be neglected. The radiation condition would also cause some difficulty here since it would require,

$$\frac{(\epsilon_o)_M}{(\epsilon_o)_P} = \frac{L_P}{L_M} \tag{5.22}$$

As the prototype usually operates at high emissivity, $(\epsilon_o)_P > .5$, coating the model with an efficient radiator $(\epsilon_o)_M \approx 1$ would not achieve much in the way of scale ratio. Since radiation is a significant mode of heat transfer here, one must resort to one of the circumventions mentioned in Section 3.1. These were to consider steady state heat transfer, to consider different temperatures and materials for model and prototype, or to go to the q_{NET} concept--i.e., the incomplete aeroelastic testing of Section 5.1e.

Utilizing this incomplete aeroelastic testing technique the similarity parameters at high Mach numbers for the same materials at the same temperatures become basically (see Eq. 5.19)

$$q_{NET}L, \ \frac{t_o}{L^2}, \ p_\infty U^2, \ \frac{u_o}{L}, \ \frac{t_o}{L}, \ \sigma_o, \ \frac{Ut_o}{L}, \ \gamma \tag{5.23}$$

where some estimate of the net heating rate, $q_{NET} = q_A - \epsilon_w \sigma T_w^4 + q_F$ would have to be made for both the prototype and model, and the wind tunnel then would be adjusted to conform with this. Additional heating by radiant heaters might be used in the tunnel if the tunnel air is not sufficient to provide the desired heating rates. The distribution of the heating rate over the model might be difficult to simulate accurately by these artificial means. Notice that this incomplete aeroelastic testing can also satisfy the time conditions t_o/L and Ut_o/L for dynamic aeroelastic tests by having U the same for model and prototype.

5.3 Application to Ballistic Missiles

The ballistic missile is generally a blunt nosed, wingless vehicle that experiences a very high but short duration aerodynamic heating rate over its trajectory. This heating occurs mainly in the vicinity of the stagnation point and is apt to be small elsewhere. Ablation is usually the primary means of thermal protection for this type of vehicle and radiation does not play a large role. The parameters of Eqs. (5.5) and (5.6) would then be appropriate. Considering first the case of the same materials at the same temperatures, Eq. (5.6) yields the following significant parameters for matching

$$\sqrt{\rho_\infty U L \mu_s}\ h_s\ ,\ \frac{Ut_o}{L}\ ,\ \frac{t_o}{L^2}\ ,\ \frac{L}{U}\ ,\ \rho_\infty U^2 L^2$$
$$V_o L\ ,\ \rho_\infty U^2\ ,\ \frac{u_o}{L}\ ,\ \frac{t_o}{L}\ ,\ \sigma_o \qquad (5.24)$$

the others being somewhat secondary (radiation, gravity effects, $T_s \gg T_w$, etc.). It is immediately seen that there is difficulty in reconciling two of the ablation parameters

(fourth and fifth) with the heating (first) and aeroelastic (seventh) requirements here. It appears then that detailed ablation similarity for these cases cannot be maintained. As mentioned in Section 3.2, however, these parameters relate to the flow of the liquid layer. If this is removed very quickly or if the ablation is essentially a sublimation type process, these parameters would not appear and hence may be neglected. There is also some difficulty in matching the unsteady aerodynamic condition Ut_o/L together with the structural dynamics condition t_o/L without going to the same velocity U. For static aeroelastic type phenomena, both of these conditions could be neglected. The similarity parameters then appear to be the same as in the Boost Glide case, Eq. (5.20), without the radiation term $\epsilon_o L$. The matching of these conditions is achieved in the same manner and results in Eq. (5.21) as before.

Alternatively, one could go to the incomplete aerothermoelastic testing procedure of Section 5.1e where $p_{NET} = \rho_\infty U^2 \bar{p}$. Application of this results in the following basic similarity parameters at high Mach numbers for the same materials at the same temperatures given by Eq. (5.19).

$$q_{NET} L \;,\; \frac{t_o}{L^2} \;,\; \frac{\gamma_A L}{V_o} \;,\; \frac{L}{V_o} \;,\; V_o L \;,\; \rho_\infty U^2$$
$$\frac{u_o}{L} \;,\; \frac{t_o}{L} \;,\; gL \;,\; \sigma_o \;,\; \gamma \;,\; \frac{Ut_o}{L} \qquad (5.25)$$

where again some estimate of the net heating rate,

$$q_{NET} = q_A - \epsilon_w \sigma T_w^4 - \dot{m}_v \eta (h_s - h_v) + q_F \qquad (5.26)$$

would have to be made, and the tunnel adjusted to conform to this. The third, fourth, and fifth parameters again refer to the melt layer and might be neglected under appropriate circumstances. Also the time conditions Ut_0/L and t_*/L for dynamic aeroelastic tests can be satisfied by having U the same for model and prototype.

6. CONSIDERATION OF TESTING FACILITIES

The parameters of the preceding sections indicate that a hypersonic wind tunnel testing facility should in general have the following capabilities:

a) high free stream enthalpy
b) high free stream velocity
c) high stagnation pressure
d) large test section
e) relatively long testing time

For a general aerothermoelastic test duplicating the aerodynamic, heat transfer, and structural phenomena of a prototype exactly, it has been shown that a full scale model must be tested in a flow with the same U, ρ_∞, T_∞ and p_∞. Thus for full scale similitude, each of the capabilities listed above is required. An indication of the operating wind tunnel stagnation temperatures and pressures (in the reservoir) necessary for duplicating these flight parameters (U, ρ_∞, T_∞, p_∞) is given in Fig. 4 (Ref. 31). For example, operating tunnel stagnation temperatures as high as 12,000°R and operating tunnel stagnation pressures as high as 10,000 atm may be required for flight duplication. It may be noted from this figure that the tunnel requirements for the ballistic missile, whose altitude range of interest is below 100,000 ft., are generally more severe than those of the boost glide vehicle, which has an altitude range of interest between 100,000 and 200,000 ft. The high stagnation temperatures and pressures indicated in Fig. 4 introduce practical engineering problems (such as melting of the tunnel nozzle throat) so that the testing time at these elevated levels must necessarily be short. Therefore, wind tunnel testing times for ballistic trajectory studies are considerably

shorter than times for boost glide studies, placing a practical limitation upon the characteristic time scale parameter.

As an alternative to reproducing the flight parameters U, ρ_∞, T_∞ and p_∞ in an experimental facility (which are the most stringent similitude requirements), the possibility of simulating the parameters associated with the specialized phenomena discussed in the preceding sections and of utilizing the concept of incomplete aerothermoelastic testing of Section 5.1e is of interest.

The pressure distribution about blunt bodies in hypersonic flow (Eq. 2.6) is seen to depend primarily on geometric similarity (β) provided the flow Mach number is approximately 3 or greater. No condition is imposed on Re_s (and consequently on L) or on ambient free stream conditions. Therefore the pertinent tunnel capability requirement here for similitude of p/p_s is simply that M_∞ be greater than approximately 3. Conventional blow-down hypersonic wind tunnels which can simulate M_∞ up to approximately 10 are thus adequate here. Gases other than air, such as helium, may also be utilized here since the effect of γ is absorbed in p_s (Eq. 2.7). Heat transfer studies about blunt bodies however introduce the additional requirement of a high enthalpy airstream (h_s) along with a consideration of Re_s (Eq. 2.31). The shock tube, which is capable of producing a high enthalpy, low M_∞ flow has been used extensively for this purpose. This facility is capable of reproducing enthalpies corresponding to near satellite velocities (Fig. 5). Hypersonic wind tunnels on the other hand are limited in this respect in that they can reproduce flight enthalpies corresponding to $M_\infty \approx 8$ only with the aid of special heaters. Ordinarily, however, these tunnels are limited to stagnation temperatures of about 1000°F, corresponding to flight at approximately

$M_\infty \approx 3.5$ in the stratosphere. The principal limitations of the shock tube are its extremely short testing time (under 1 millisecond) and small test section, whereas the blowdown tunnels have large test sections and times up to about one minute.

Pressure distribution studies about slender bodies (Section 2.2) require facilities with a higher Mach number capability than is generally necessary for blunt body experiments. Here again hypersonic wind tunnels are useful for inviscid pressure experiments where the pertinent flow parameters are $M\gamma, M^3 k \frac{d}{L}, \gamma$. Mach numbers up to approximately 15 (using air) can be reproduced (Fig. 5) at the corresponding stagnation temperatures required to prevent condensation.* Still higher Mach numbers ($M_\infty \approx 20$) can be achieved with helium tunnels where condensation is not a problem. Some latitude in scaling is possible here since γ and d may be adjusted within certain practical limits. Note that there is no condition on the length scale L here since there is no requirement on Re_s . Viscous interaction effects and heat transfer studies introduce the additional considerations of stagnation temperature and Re_s (Eqs. 2.14 and 2.37). The blow-down wind tunnel, as already indicated, is limited with respect to stagnation temperature but may be used for the lower velocity region of the boost glide trajectory, and shock tubes are limited with respect to Mach number. Higher enthalpies and Mach numbers are possible in the shock tube tunnel (Ref. 31) which expands the high enthalpy flow of the shock tube through a nozzle. Fig. 6, for example, illustrates the operating range of the Cornell Aeronautical Laboratory's 24 inch shock tube tunnel. Mach numbers up to approximately 20, stagnation pressures up to about 400 atmospheres and stagnation temperatures as high as 6200°F, may be achieved in this tunnel. The shock tube

*Flight stagnation temperatures will not be reproduced here, however, for M greater than about 8.

tunnel thus has the capability of reproducing the required aerodynamic parameters associated with a major portion of both boost glide and ballistic missile trajectories in reasonably large test sections. As with the shock tube, the shock tube tunnel is limited with regard to testing time (order of 5 to 15 milliseconds).

Another facility which makes use of shock wave heating to produce high enthalpy flow at high M_∞ and high stagnation pressures is the Wave Superheater being developed at Cornell Aeronautical Laboratory (Ref. 32). Mach numbers of 5 to 15 and air temperatures between 5000°R and 10,000°R are possible for flow durations up to approximately 30 seconds.

Very high stagnation enthalpies and Mach numbers, corresponding to ballistic trajectory values are also possible in the arc-discharge or "hotshot" wind tunnels. Reynolds numbers are an order of magnitude greater than those produced by shock tunnels but running times are only slightly greater. These tunnels are particularly suitable for high M_∞ , high enthalpy flows and their chief disadvantage, in addition to short running times, is the contamination of the flow due to the arc burning process.

Inevitably, recourse must be made to incomplete aerothermoelastic testing as discussed in Section 5.1e. As already indicated there, it is generally more difficult to artificially apply the aerodynamic pressure environment than the heat transfer environment, particularly for dynamic aeroelastic type tests. An estimate of each is first necessary. The pressure and heat transfer environments however may be adequately estimated in static type situations by utilizing experiments conducted in the facilities discussed earlier in this section, such as the shock tube tunnel for example, in conjunction with theoretical estimates. With

this information, tests which are intended primarily for the study of structural and material behavior and which require large test sections and long running times, may be conducted in facilities such as rocket exhausts, plasma jets, radiant heaters, etc. These latter facilities are particularly attractive because of the high thermal fluxes which they can provide.

The development of rarefied gas flow facilities has lagged the continuum flow facilities. Presently operating low density wind tunnels are capable of producing velocities of about 2500 ft/sec. and Mach numbers up to about 6. Facilities are planned to extend this range to Mach numbers of approximately 10 (Ref. 33). Some typical tests on cylinders conducted in low density wind tunnels are reported in Refs. 13, 11 and 34. Knudsen numbers as high as 185 (Ref. 13) and molecular speed ratios of the order of 2 to 3 were achieved. Tests of a different nature using a model supported by an arm revolving at high speed in a vacuum chamber are described in Ref. 35. The pressure in the chamber was varied and molecular speed ratios of approximately 1.5 were attained.

The regions of simulation of some typical aerodynamic facilities are indicated in Fig. 5 along with typical boost-glide and ballistic missile trajectories (Ref. 33).

7. SUMMARY AND CONCLUSIONS

The present report has derived the similarity parameters required for aerothermoelastic studies at Mach numbers extending into the hypersonic regime. This study has considered in detail the external pressure and heat flux imposed upon the structure, the heat transfer distribution within the structure (for both ablating and non-ablating materials) and the stress deflection behavior under short time and long time loading conditions.

Similitude for the general hypersonic aerothermoelastic problem is not possible and a model must be an identical size replica of the prototype with the same pressure and thermal environments. Although the Mach number does not play a dominant role here, the basic conflict in similitude arises from mutually satisfying the requirements of same temperature T, Reynolds number Re_s, radiation parameter $\epsilon_o T_o^3 L/K_o$, and the aeroelastic parameter $\rho_\infty U^2/E_o$.

Certain relaxations of this basic conflict are possible when considering specialized situations. This has been brought out in the parameters which apply specifically to blunt bodies and affinely related slender bodies. These specialized situations were examined for both continuum and free molecule flow. Even though these specialized situations offer some relaxation, the problem of similitude is still extremely difficult because of the high operating temperatures and the attendant problems of creep and fatigue. Recourse may then be made to "incomplete aerothermoelastic testing" in which the pressure and thermal loadings must be

estimated in advance and applied artificially to the model. Otherwise it appears that only "restricted purpose" models investigating some specific problem such as aerodynamic pressure, aerodynamic heating, heat conduction, or stress and deflection behavior, separately is the only other alternative here, rather than a complete aerothermoelastic model.

REFERENCES

1. Calligeros, J. M., and Dugundji, J., Similarity Laws Required for Experimental Aerothermoelastic Studies, MIT ASRL TR 75-1, May 1959.

2. Hayes, W. D., and Probstein, R. F., Viscous Hypersonic Similitude, Journal of the Aero/Space Sciences, Vol. 26, No. 12, December 1959.

3. Lees, L., Hypersonic Flow, JAS-RAeS Fifth International Aeronautical Conference, Los Angeles, Preprint 554, June 20-24, 1955.

4. Series of Articles on Hypersonic Flow, Journal of the Royal Aeronautical Society, Vol. 63, No. 585, September 1959.

5. Tsien, H. S., Similarity Law of Hypersonic Flow, Journal of Mathematics and Physics, Vol. 25, pp 247-251, 1946.

6. Hayes, W. D., On Hypersonic Similitude, Quarterly of Applied Mathematics, Vol. 5, pp 105-106, 1947.

7. Bertram, M. H., and Henderson, A., Jr., Effects of Boundary-Layer Displacement and Leading-Edge Bluntness on Pressure Distribution, Skin Friction, and Heat Transfer of Bodies at Hypersonic Speeds, NACA TN 4301, July 1958.

8. Cheng, H. K., Similitude of Hypersonic Real-Gas Flows Over Slender Bodies With Blunted Noses, Journal of the Aero/Space Sciences, Vol. 26, No. 9, September 1959.

9. Lees, L., and Kubota, T., Inviscid Hypersonic Flow Over Blunt-Nosed Slender Bodies, Journal of the Aeronautical Sciences, Vol. 24, No. 3, March 1957.

10. Tsien, H. S., Superaerodynamics, Mechanics of Rarefied Gases, Journal of the Aeronautical Sciences, Vol. 13, No. 12, December 1946.

11. Stalder, J. R., Goodwin, G., and Creager, M. O., Heat Transfer to Bodies in a High-Speed Rarefied-Gas Stream, NACA Report 1093, 1952.

12. Ashley, H., Application of the Theory of Free Molecule Flow to Aeronautics, Journal of the Aeronautical Sciences, Vol. 16, No. 2, February 1949.

13. Stalder, J. R., Goodwin, G., and Creager, M. O, A Comparison of Theory and Experiment for High-Speed Free-Molecule Flow, NACA Report 1032, 1951.

14. Stalder, J. R., and Zurick, V. J., Theoretical Aerodynamic Characteristics of Bodies in a Free-Molecule-Flow Field, NACA TN 2423, July 1951.

15. Fay, J. A., and Riddell, F. R., Theory of Stagnation Point Heat Transfer in Dissociated Air, Journal of the Aeronautical Sciences, Vol. 25, No. 2, February 1958.

16. Goulard, R., On Catalytic Recombination Rates in Hypersonic Stagnation Heat Transfer, Jet Propulsion,Vol. 28, No. 11, November 1958.

17. Kemp, N. H., and Riddell, F. R., Heat Transfer to Satellite Vehicles Re-entering the Atmosphere, Jet Propulsion, Vol. 27, No. 2, February 1957.

18. Kemp, N. H., Rose, P. H., and Detra, R. W., Laminar Heat Transfer Around Blunt Bodies in Dissociated Air, Journal of the Aero/Space Sciences, Vol. 26, No. 7, July 1959.

19. Rose, P. H., Probstein, R. F., and Adams, M. C., Turbulent Heat Transfer Through a Highly Cooled Partially Dissociated Boundary Layer, Journal of the Aero/Space Sciences, Vol. 25, No. 12, December 1958.

20. Hayes, W. D., and Probstein, R. F., Hypersonic Flow Theory, Academic Press, New York, 1959.

21. Heldenfels, R. R., and Rosecrans, R., Preliminary Results of Supersonic-Jet Tests of Simplified Wing Structures, NACA RM L53E26a, July 1953.

22. Budiansky, B., and Mayers, J., Influence of Aerodynamic Heating on the Effective Torsional Stiffness of Thin Wings, Journal of the Aeronautical Sciences, Vol. 23, No. 12, December 1956.

23. Bethe, H. A., and Adams, M. C., A Theory for the Ablation of Glassy Materials, Journal of the Aero/Space Sciences, Vol. 26, No. 6, June 1959.

24. Sutton, G. W., The Hydrodynamics and Heat Conduction of a Melting Surface, Journal of the Aeronautical Sciences, Vol. 25, No. 1, January 1958.

25. Lees, L., Similarity Parameters for Surface Melting of a Blunt Nosed Body in a High Velocity Gas Stream, Journal of the American Rocket Society, Vol. 29, No. 5, May 1959.

26. Adams, M. C., Recent Advances in Ablation, ARS Journal, Vol. 29, No. 9, September 1959.

27. Gatewood, B. E., Thermal Stresses, McGraw-Hill Book Company, Inc., New York, 1957.

28. Gerard, G., Some Structural Aspects of Thermal Flight, Paper presented at the Aviation Division of the ASME Symposium on the Thermal Barrier, November 28 - December 3, 1954.

29. Shanley, F. R., Strength of Materials, McGraw-Hill Book Company, Inc., New York, 1957.

30. Grover, H. J., Gorden, S. A., and Jackson, L. R., Fatigue of Metals and Structures, Bureau of Aeronautics NAVAER 00-25-534, 1954.

31. Hertzberg, A., and Wittliff, C. E., Studying Hypersonic Flight in the Shock Tunnel, IAS Paper No. 60-67, Presented at the IAS National Summer Meeting, Los Angeles, California June 28 - July 1, 1960.

32. Weatherston, R. C., Hypersonic Flight in the Laboratory, Research Trends, Cornell Aeronautical Laboratory, Vol. VII, No. 2, 1959.

33. Lukasiewicz, J., Experimental Investigation of Hypersonic Flight, Advances in Aeronautical Sciences, Proceedings of the First International Congress in the Aeronautical Sciences, Madrid, September 8-13, 1958, Vol. I, Pergamon Press 1959.

34. Cybulski, R. J., and Baldwin, L. V., Heat Transfer from Cylinders in Transition from Slip Flow to Free-Molecule Flow, NASA MEMO 4-27-59E, May 1959.

35. Devienne, F. M., Experimental Study of the Stagnation Temperature in a Free Molecular Flow, Journal of the Aeronautical Sciences, Vol. 24, No. 6, June 1957.

36. Martin, J. F., New Tool for Research, Research Trends, Cornell Aeronautical Laboratory, Vol. VII, No. 4, 1960.

37. Trussell, D. H., and Weidman, D. J., A Radiant Heater to Simulate Aerodynamic Heating in a Wind Tunnel, NASA TN D-530, November 1960.

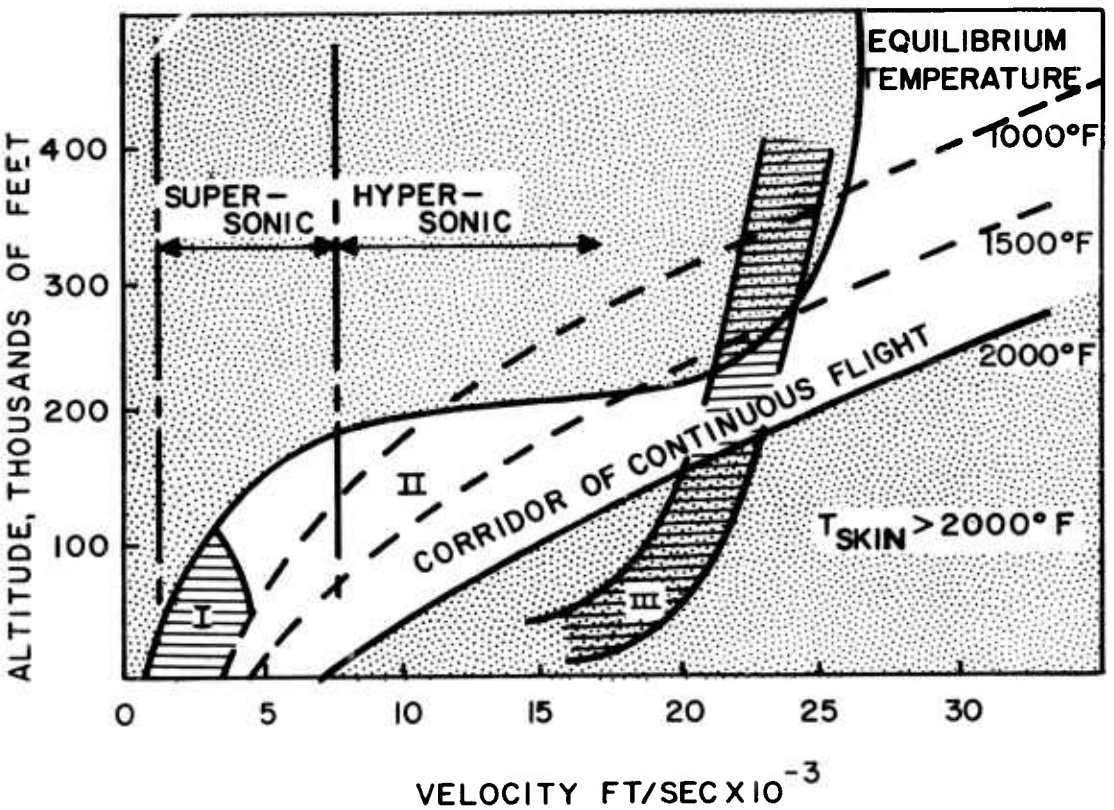

FIG. 1 CORRIDOR OF CONTINUOUS FLIGHT

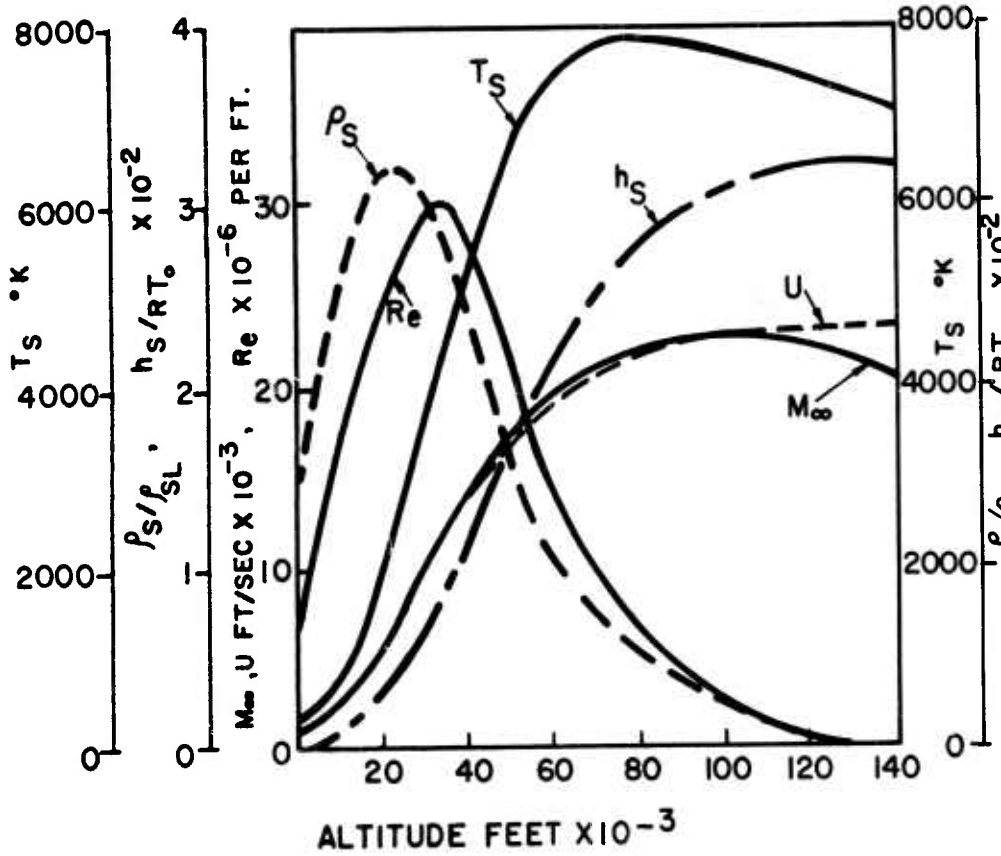

FIGURE 2a. TYPICAL AERODYNAMIC CONDITIONS FOR A BALLISTIC MISSILE.
(RANGE = 6,000 MILES, U_ε = 23,000 FT / SEC)

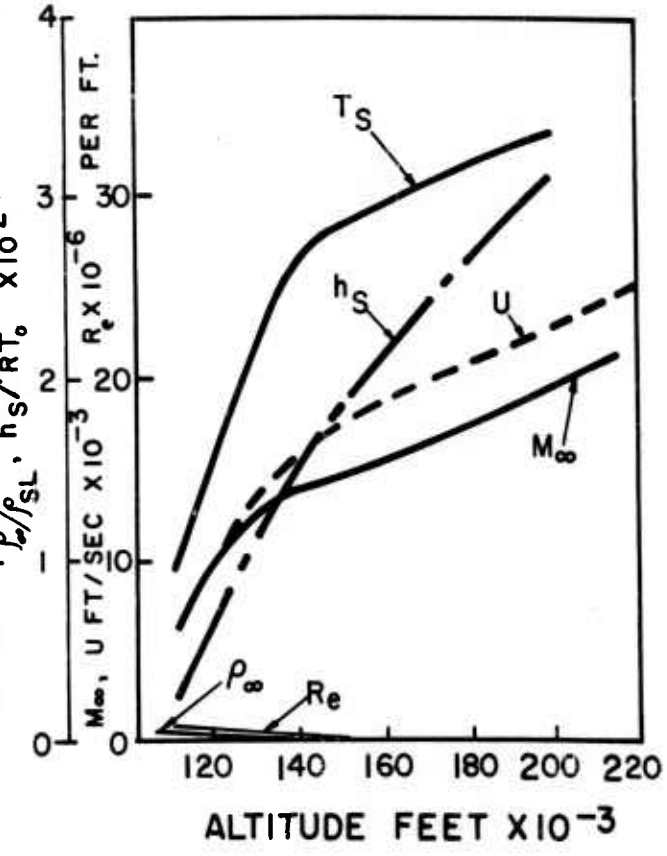

FIGURE 2b. TYPICAL AERODYNAMIC CONDITIONS FOR A GLIDE VEHICLE.
($\frac{L}{D}$ = 5, W/S = 20 lb/FT^2)

TAKEN FROM REF. 4

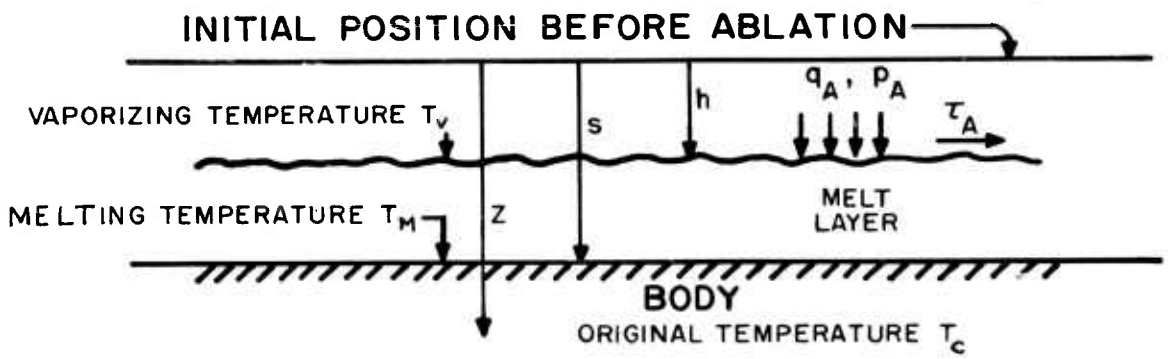

FIGURE 3. COORDINATE SYSTEM FOR ABLATING BODY.

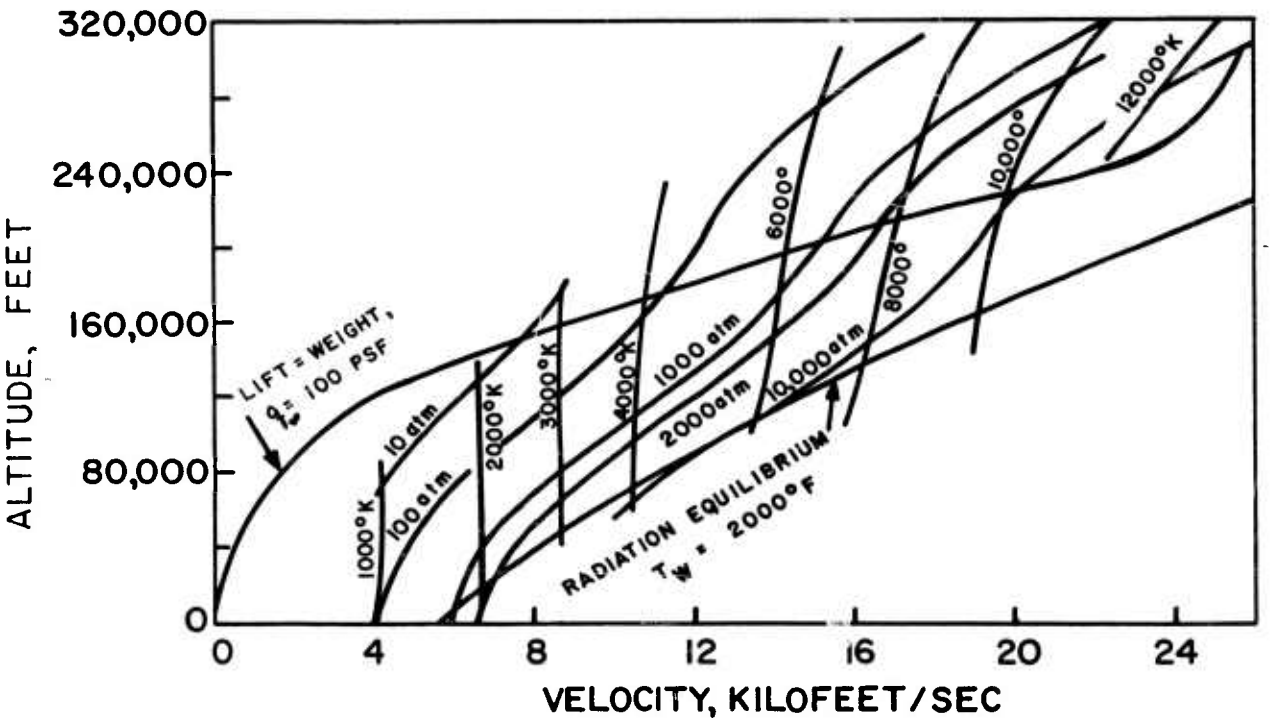

FIGURE 4. TUNNEL STAGNATION PRESSURES AND STAGNATION TEMPERATURES REQUIRED FOR FLIGHT DUPLICATION.

Taken From Ref. 31

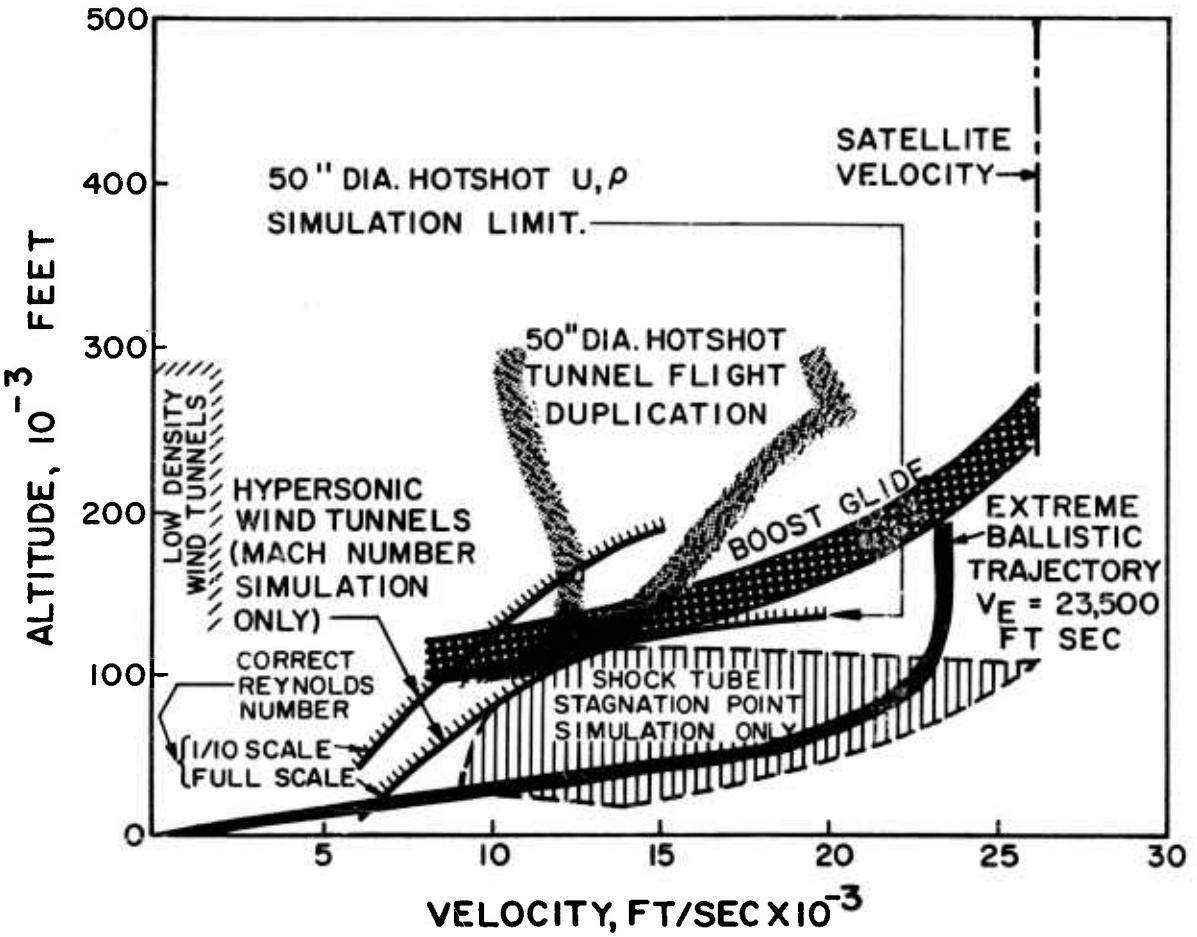

FIG.5 TYPICAL TRAJECTORIES AND REGIONS OF SIMULATION.

TAKEN FROM REF. 33

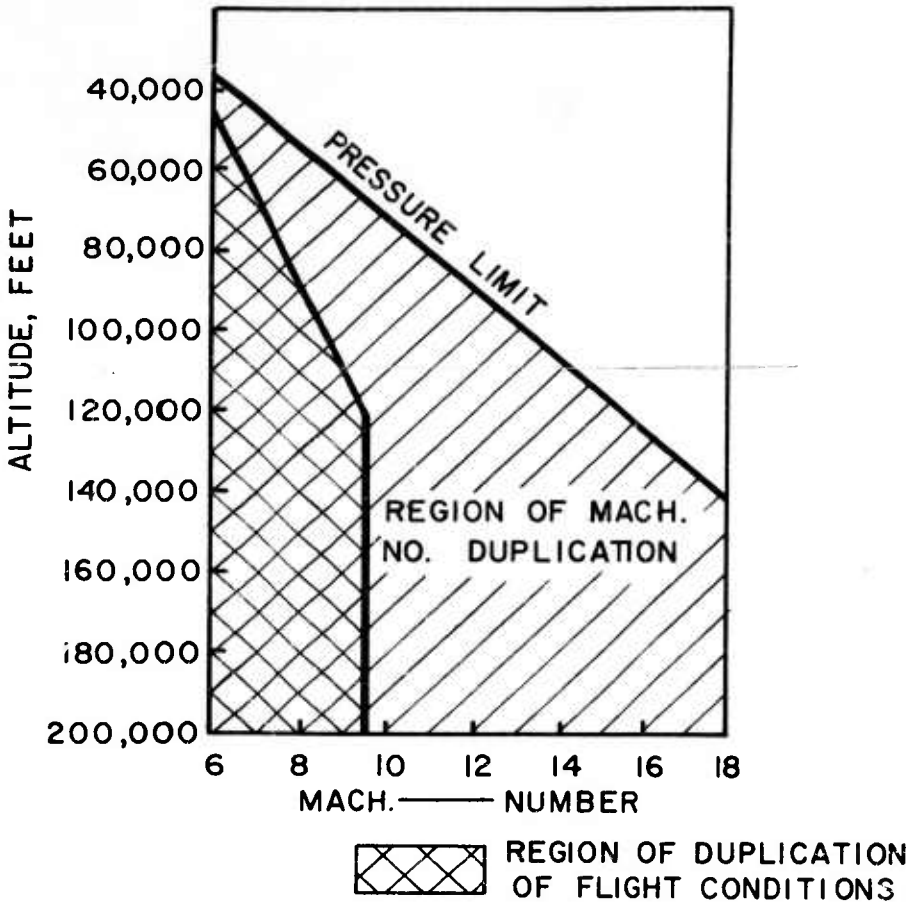

FIGURE 6

OPERATING RANGE OF CORNELL AERONAUTICAL LABORATORY'S 24 INCH SHOCK TUNNEL.

TAKEN FROM REF. 36